J|A|C|S
ARTICLES
Published on Web 01/30/2004

Probing the Ruthenium−Cumulene Bonding Interaction: Synthesis and Spectroscopic Studies of Vinylidene− and Allenylidene−Ruthenium Complexes Supported by Tetradentate Macrocyclic Tertiary Amine and Comparisons with Diphosphine Analogues of Ruthenium and Osmium†

Chun-Yuen Wong, Chi-Ming Che,* Michael C. W. Chan, King-Hung Leung, David Lee Phillips,* and Nianyong Zhu

Contribution from the Department of Chemistry and HKU-CAS Joint Laboratory on New Materials, The University of Hong Kong, Pokfulam Road, Hong Kong SAR, China

Received August 22, 2003; E-mail: cmche@hku.hk

Abstract: The synthesis and spectroscopic properties of *trans*-[Cl(16-TMC)Ru=C=CHR]PF_6 (16-TMC = 1,5,9,13-tetramethyl-1,5,9,13-tetraazacyclohexadecane, R = C_6H_4X-4, X = H (**1**), Cl (**2**), Me (**3**), OMe (**4**); R = $CHPh_2$ (**5**)), *trans*-[Cl(16-TMC)Ru=C=C=C(C_6H_4X-4)$_2$]PF_6 (X = H (**6**), Cl (**7**), Me (**8**), OMe (**9**)), and *trans*-[Cl(dppm)$_2$M=C=C=C(C_6H_4X-4)$_2$]PF_6 (M = Ru, X = H (**10**), Cl (**11**), Me (**12**); M = Os, X = H (**13**), Cl (**14**), Me (**15**)) are described. The crystal structures of **1**, **5**, **6**, and **8** show that the Ru−C_α and C_α−C_β distances of the allenylidene complexes fall between those of the vinylidene and acetylide relatives. Two reversible redox couples are observed by cyclic voltammetry for **6**−**9**, with $E_{1/2}$ values ranging from −1.19 to −1.42 and 0.49 to 0.70 V vs $Cp_2Fe^{+/0}$, and they are both 0.2−0.3 and 0.1−0.2 V more reducing than those for **10**−**12** and **13**−**15**, respectively. The UV−vis spectra of the vinylidene complexes **1**−**4** are dominated by intense high-energy bands at $\lambda_{max} \leq 310$ nm ($\epsilon_{max} \geq 10^4$ dm^3 mol^{-1} cm^{-1}), while weak absorptions at $\lambda_{max} \geq 400$ nm ($\epsilon_{max} \leq 10^2$ dm^3 mol^{-1} cm^{-1}) are tentatively assigned to d−d transitions. The resonance Raman spectrum of **5** contains a nominal $\nu_{C=C}$ stretch mode of the vinylidene ligand at 1629 cm^{-1}. The electronic absorption spectra of the allenylidene complexes **6**−**9** exhibit an intense absorption at λ_{max} = 479−513 nm (ϵ_{max} = (2−3) × 10^4 dm^3 mol^{-1} cm^{-1}). Similar electronic absorption bands have been found for **10**−**12**, but the lowest energy dipole-allowed transition is blue-shifted by 1530−1830 cm^{-1} for the Os analogues **13**−**15**. Ab initio calculations have been performed on the ground state of *trans*-[Cl-$(NH_3)_4$Ru=C=C=CPh_2]$^+$ at the MP2 level, and imply that the HOMO is not localized purely on the metal center or allenylidene ligand. The absorption band of **6** at λ_{max} = 479 nm has been probed by resonance Raman spectroscopy. Simulations of the absorption band and the resonance Raman intensities show that the nominal $\nu_{C=C=C}$ stretch mode accounts for ca. 50% of the total vibrational reorganization energy, indicating that this absorption band is strongly coupled to the allenylidene moiety. The excited-state reorganization of the allenylidene ligand is accompanied by rearrangement of the Ru=C and Ru−N (of 16-TMC) fragments, which supports the existence of bonding interaction between the metal and C=C=C unit in the electronic excited state.

Introduction

The chemistry of metallacumulenes M(=C)$_n$$CR_2$ is of considerable interest from several perspectives.[1] In the context of materials science, π-conjugated linear (=C)$_n$ moieties fundamentally allow communication between metal centers and remote functional groups, and potential applications as nonlinear optical materials and molecular wires have been advocated.[2] Metallacumulenes also represent an interesting class of metal−carbon multiple-bonded compounds for the study of the bonding interaction in M(=C)$_n$$CR_2$, particularly with regard to the oxidation state assignment of the metal ion and the degree of π-bonding/back-bonding interaction. Extensive synthetic investigations and numerous X-ray structural determinations, theoretical calculations, and vibrational mode studies have been undertaken for metallacumulenes.[3] The majority of these complexes are supported by phosphine and/or cyclopentadienyl ligands, while P,O-[4] and N-chelating[5] groups have also been described.

† In memory of Dr. Vincent M. Miskowski.

* For correspondence regarding Raman spectroscopy: phillips@hku.hk.

(1) (a) Bruce, M. I. *Chem. Rev.* **1998**, *98*, 2797−2858. (b) Bruce, M. I. *Chem. Rev.* **1991**, *91*, 197−257.

(2) (a) Hurst, S. K.; Cifuentes, M. P.; Morrall, J. P. L.; Lucas, N. T.; Whittall, I. R.; Humphrey, M. G.; Asselberghs, I.; Persoons, A.; Samoc, M.; Luther-Davies, B.; Willis, A. C. *Organometallics* **2001**, *20*, 4664−4675. (b) Uno, M.; Dixneuf, P. H. *Angew. Chem., Int. Ed. Engl.* **1998**, *37*, 1714−1717. (c) Lang, H. *Angew. Chem., Int. Ed. Engl.* **1994**, *33*, 547−550. Examples of other metal analogues and acetylide relatives: (d) McDonagh, A. M.; Humphrey, M. G.; Samoc, M.; Luther-Davies, B.; Houbrechts, S.; Wada, T.; Sasabe, H.; Persoons, A. *J. Am. Chem. Soc.* **1999**, *121*, 1405−1406. (e) Bartik, T.; Weng, W.; Ramsden, J. A.; Szafert, S.; Falloon, S. B.; Arif, A. M.; Gladysz, J. A. *J. Am. Chem. Soc.* **1998**, *120*, 11071−11081.

10.1021/ja0380648 CCC: $27.50

Due to their conjugated nature, the bonding of metallacumulenes may be represented by mesomeric structures, such as $M^{-}-C\equiv C-C^{+}R_2 \leftrightarrow M=C=C=CR_2$, for allenylidene complexes.[6] To facilitate the development of these materials, particularly for optoelectronic applications, it is important to understand the excited states arising from the electronic transitions associated with $M(=C)_nCR_2$ moieties. Techniques such as UV−vis and resonance Raman spectroscopy can be employed to investigate the properties of such excited states, and they can also provide information regarding the interaction between the metal and cumulene ligand in both the ground and excited states. However, there have been few spectroscopic studies on metallacumulenes, and the ubiquitous incorporation of unsaturated organic ancillary ligands in $M(=C)_nCR_2$ complexes has hampered spectral assignment and interpretation.

We are interested in ruthenium−carbon multiple-bonded complexes, which have been established as novel and diverse catalysts for important organic transformations.[7] For example, the Grubbs alkylidene complexes $RuCl_2(=CHR)(PR_3)_2$ and more recent congeners containing N-heterocyclic carbene ligands are highly active and functional-group-tolerant catalysts for olefin metathesis reactions.[8] Ruthenium−carbene species have been proposed as active intermediates for carbene insertions into C=C and C−H bonds, as highlighted by reports on ruthenium−porphyrin catalysts.[9] Ruthenium−allenylidene complexes have also recently been employed as catalysts for ring-closing olefin metathesis and propargylation of aromatic compounds.[10] Nevertheless, despite their demonstrated capabilities and versatility, investigations regarding the spectroscopic nature of Ru=C moieties remain sparse in the literature. We recently initiated research activities for organoruthenium complexes containing the macrocyclic tertiary amine 1,5,9,13-tetramethyl-1,5,9,13-tetraazacyclohexadecane (16-TMC).[5d,11] This ligand is optically transparent in the UV−vis spectral region and is ideally suited to allow examination of the electronic transitions associated with the $Ru(=C)_nCR_2$ fragment. Furthermore, 16-TMC is a pure σ-donor and does not compete with the $(=C)_nCR_2$ ligand for π-bonding (either direct $d_\pi-p_\pi$ (filled) or π-back-bonding) interactions. This and closely related macrocyclic ligands have been widely used to stabilize metal−oxygen and −nitrogen multiple-bonded systems.[12]

Previous reports have shown that stable oxoruthenium(IV) and -(VI) complexes of 16-TMC can be obtained at relatively low reduction potentials.[13] In this account, we prepared a series of aryl-substituted vinylidene− and allenylidene−ruthenium complexes supported by 16-TMC. Rational methodologies toward the targeted organometallic species have been devised, and a hydrogen-atom addition reaction by the allenylidene complexes is also described. To provide a comparative study on the ligand effect upon the spectroscopic and electrochemical properties of the $[Ru=C=C=CR_2]$ moiety, $(dppm)_2$-ligated ruthenium and osmium congeners have also been prepared and investigated. Theoretical calculations on the ground state of the model complex $[Cl(NH_3)_4Ru=C=C=CPh_2]^+$ have been performed. Resonance Raman spectroscopy has been utilized to probe the electronic transitions associated with the vinylidene and allenylidene complexes in order to gain insight into the nature of the $Ru(=C)_nCR_2$ bonding interaction.

Experimental Section

General Procedures. All reactions were performed under a nitrogen atmosphere using standard Schlenk techniques unless otherwise stated. All reagents were used as received, and solvents were purified by

(3) For examples, see: (a) Ilg, K.; Werner, H. *Chem. Eur. J.* **2002**, *8*, 2812−2820. (b) Rigaut, S.; Monnier, F.; Mousset, F.; Touchard, D.; Dixneuf, P. H. *Organometallics* **2002**, *21*, 2654−2661. (c) Bustelo, E.; Jiménez-Tenorio, M.; Mereiter, K.; Puerta, M. C.; Valerga, P. *Organometallics* **2002**, *21*, 1903−1911. (d) Cadierno, V.; Conejero, S.; Gamasa, M. P.; Gimeno, J.; Rodríguez, M. A. *Organometallics* **2002**, *21*, 203−209. (e) Cadierno, V.; Gamasa, M. P.; Gimeno, J.; González-Bernardo, C.; Pérez-Carreño, E.; García-Granda, S. *Organometallics* **2001**, *20*, 5177−5188. (f) González-Herrero, P.; Weberndörfer, B.; Ilg, K.; Wolf, J.; Werner, H. *Organometallics* **2001**, *20*, 3672−3685. (g) Moigno, D.; Kiefer, W.; Callejas-Gaspar, B.; Gil-Rubio, J.; Werner, H. *New J. Chem.* **2001**, *25*, 1389−1397. (h) Bruce, M. I.; Low, P. J.; Costuas, K.; Halet, J.-F.; Best, S. P.; Heath, G. A. *J. Am. Chem. Soc.* **2000**, *122*, 1949−1962. (i) Re, N.; Sgamellotti, A.; Floriani, C. *Organometallics* **2000**, *19*, 1115−1122. (j) Moigno, D.; Kiefer, W.; Gil-Rubio, J.; Werner, H. *J. Organomet. Chem.* **2000**, *612*, 125−132. (k) Touchard, D.; Haquette, P.; Daridor, A.; Romero, A.; Dixneuf, P. H. *Organometallics* **1998**, *17*, 3844−3852. (l) Colbert, M. C. B.; Lewis, J.; Long, N. J.; Raithby, P. R.; Younus, M.; White, A. J. P.; Williams, D. J.; Payne, N. N.; Yellowlees, L.; Beljonne, D.; Chawdhury, N.; Friend, R. H. *Organometallics* **1998**, *17*, 3034−3043. (m) Touchard, D.; Dixneuf, P. H. *Coord. Chem. Rev.* **1998**, *178*−*180*, 409−429. (n) Oliván, M.; Eisenstein, O.; Caulton, K. G. *Organometallics* **1997**, *16*, 2227−2229. (o) Werner, H. *Chem. Commun.* **1997**, 903−910.

(4) (a) Martín, M.; Gevert, O.; Werner, H. *J. Chem. Soc., Dalton Trans.* **1996**, 2275−2283. (b) Braun, T.; Steinert, P.; Werner, H. *J. Organomet. Chem.* **1995**, *488*, 169−176.

(5) (a) Rüba, E.; Hummel, A.; Mereiter, K.; Schmid, R.; Kirchner, K. *Organometallics* **2002**, *21*, 4955−4959. (b) Tenorio, M. A. J.; Tenorio, M. J.; Puerta, M. C.; Valerga, P. *Organometallics* **2000**, *19*, 1333−1342. (c) Cadierno, V.; Gamasa, M. P.; Gimeno, J.; Iglesias, L.; García-Granda, S. *Inorg. Chem.* **1999**, *38*, 2874−2879. (d) Yang, S.-M.; Chan, M. C. W.; Cheung, K.-K.; Che, C.-M.; Peng, S.-M. *Organometallics* **1997**, *16*, 2819−2826. (e) Slugovc, C.; Mereiter, K.; Zobetz, E.; Schmid, R.; Kirchner, K. *Organometallics* **1996**, *15*, 5275−5277.

(6) (a) Tamm, M.; Jentzsch, T.; Werncke, W. *Organometallics* **1997**, *16*, 1418−1424. (b) Bruce, M. I.; Hinterding, P.; Low, P. J.; Skelton, B. W.; White, A. H. *Chem. Commun.* **1996**, 1009−1010. (c) Touchard, D.; Pirio, N.; Toupet, L.; Fettouhi, M.; Ouahab, L.; Dixneuf, P. H. *Organometallics* **1995**, *14*, 5263−5272.

(7) (a) Trost, B. M.; Toste, F. D.; Pinkerton, A. B. *Chem. Rev.* **2001**, *101*, 2067−2096. (b) Naota, T.; Takaya, H.; Murahashi, S.-I. *Chem. Rev.* **1998**, *98*, 2599−2660. (c) Doyle, M. P.; Forbes, D. C. *Chem. Rev.* **1998**, *98*, 911−935. (d) Bruneau, C.; Dixneuf, P. H. *Acc. Chem. Res.* **1999**, *32*, 311−323.

(8) (a) Sanford, M. S.; Ulman, M.; Grubbs, R. H. *J. Am. Chem. Soc.* **2001**, *123*, 749−750. (b) Weskamp, T.; Kohl, F. J.; Hieringer, W.; Gleich, D.; Herrmann, W. A. *Angew. Chem., Int. Ed. Engl.* **1999**, *38*, 2416−2419. (c) Huang, J.; Stevens, E. D.; Nolan, S. P.; Petersen, J. L. *J. Am. Chem. Soc.* **1999**, *121*, 2674−2678. (d) Scholl, M.; Ding, S.; Lee, C. W.; Grubbs, R. H. *Org. Lett.* **1999**, *1*, 953−956. (e) Weskamp, T.; Schattenmann, W. C.; Spiegler, M.; Herrmann, W. A. *Angew. Chem., Int. Ed. Engl.* **1998**, *37*, 2490−2493. (f) Schwab, P.; Grubbs, R. H.; Ziller, J. W. *J. Am. Chem. Soc.* **1996**, *118*, 100−110. (g) Nguyen, S. T.; Grubbs, R. H.; Ziller, J. W. *J. Am. Chem. Soc.* **1993**, *115*, 9858−9859.

(9) (a) Li, Y.; Huang, J.-S.; Zhou, Z.-Y.; Che, C.-M.; You, X.-Z. *J. Am. Chem. Soc.* **2002**, *124*, 13185−13193. (b) Miller, J. A.; Jin, W.; Nguyen, S. T. *Angew. Chem., Int. Ed.* **2002**, *41*, 2953−2956. (c) Munslow, I. J.; Gillespie, K. M.; Deeth, R. J.; Scott, P. *Chem. Commun.* **2001**, 1638−1639. (d) Che, C.-M.; Huang, J.-S.; Lee, F.-W.; Li, Y.; Lai, T.-S.; Kwong, H.-L.; Teng, P.-F.; Lee, W.-S.; Lo, W.-C.; Peng, S.-M.; Zhou, Z.-Y. *J. Am. Chem. Soc.* **2001**, *123*, 4119−4129. (e) Li, Y.; Huang, J.-S.; Zhou, Z.-Y.; Che, C.-M. *J. Am. Chem. Soc.* **2001**, *123*, 4843−4844. (f) Hamaker, C. G.; Mirafzal, G. A.; Woo, L. K. *Organometallics* **2001**, *20*, 5171−5176. (g) Galardon, E.; Maux, P. L.; Simonneaux, G. *Tetrahedron* **2000**, *56*, 615−621. (h) Wolf, J. R.; Hamaker, C. G.; Djukic, J.-P.; Kodadek, T.; Woo, L. K. *J. Am. Chem. Soc.* **1995**, *117*, 9194−9199. (i) Smith, D. A.; Reynolds, D. N.; Woo, L. K. *J. Am. Chem. Soc.* **1993**, *115*, 2511−2513.

(10) (a) Nishibayashi, Y.; Inada, Y.; Hidai, M.; Uemura, S. *J. Am. Chem. Soc.* **2002**, *124*, 7900−7901. (b) Nishibayashi, Y.; Yoshikawa, M.; Inada, Y.; Hidai, M.; Uemura, S. *J. Am. Chem. Soc.* **2002**, *124*, 11846−11847. (c) Sémeril, D.; Oliver-Bourbigou, H.; Bruneau, C.; Dixneuf, P. H. *Chem. Commun.* **2002**, 146−147. (d) Fürstner, A.; Liebl, M.; Lehmann, C. W.; Picquet, M.; Kunz, R.; Bruneau, C.; Touchard, D.; Dixneuf, P. H. *Chem. Eur. J.* **2000**, *6*, 1847−1857.

(11) (a) Choi, M.-Y.; Chan, M. C. W.; Peng, S.-M.; Cheung, K.-K.; Che, C.-M. *Chem. Commun.* **2000**, 1259−1260. (b) Choi, M.-Y.; Chan, M. C. W.; Zhang, S.; Cheung, K.-K.; Che, C.-M.; Wong, K.-Y. *Organometallics* **1999**, *18*, 2074−2080. (c) Yang, S.-M.; Chan, M. C. W.; Peng, S.-M.; Che, C.-M. *Organometallics* **1998**, *17*, 151−155. (d) Yang, S.-M.; Cheng, W.-C.; Peng, S.-M.; Cheung, K.-K.; Che, C.-M. *J. Chem. Soc., Dalton Trans.* **1995**, 2955−2959.

(12) (a) Chan, P.-M.; Yu, W.-Y.; Che, C.-M.; Cheung, K.-K. *J. Chem. Soc., Dalton Trans.* **1998**, 3183−3190. (b) Che, C.-M.; Lai, T.-F.; Wong, K.-Y. *Inorg. Chem.* **1987**, *26*, 2289−2299. (c) Che, C.-M.; Wong, K.-Y.; Poon, C.-K. *Inorg. Chem.* **1986**, *25*, 1809−1813.

(13) Che, C.-M.; Yam, V. W.-W. *Adv. Inorg. Chem.* **1992**, *39*, 233−325.

standard methods. Zinc amalgam was prepared by adding zinc turning (0.3 g) to a methanolic solution (10 mL) of mercury acetate (0.1 g), followed by washing with methanol. $[Ru(16\text{-}TMC)Cl_2]Cl$,[12c] $RuCl_2(=CHPh)(PCy_3)_2$,[8f] $RuCl_2(=C=CHPh)(PCy_3)_2$,[14] *trans*-$[Cl(dppm)_2Ru=C=C=C(C_6H_4X\text{-}4)_2]PF_6$ (X = H, Cl, Me (**10**−**12**)),[15] and *cis*-$[Os(dppm)_2Cl_2]$[16] were prepared according to published procedures.

^1H, $^{13}C\{^1H\}$, DEPT-135, and $^{31}P\{^1H\}$ NMR spectra were recorded on Bruker 400 DPX, 500 DRX, and 600 DRX FT-NMR spectrometers. Peak positions were calibrated with solvent residue peaks as internal standard for ^1H and $^{13}C\{^1H\}$ spectra, while the ^{31}P NMR spectra were referenced to external 85% H_3PO_4. In the ^1H and $^{13}C\{^1H\}$ NMR spectra, multiple resonances corresponding to different conformations of 16-TMC were observed. This is because the 16-TMC ligand, like its congeners 14- and 15-TMC, can exhibit several possible conformations upon coordination to the metal center[12b,17] (the crystal structures in this work also show that some $(CH_2)_3$ groups are disordered, and the methyl groups attached to N atoms are often disordered and occupy at least two positions). Variable-temperature ^1H and $^{13}C\{^1H\}$ NMR spectra (−75 and 35 °C) for complex **7** have been recorded, and the minimal differences observed suggest that the conformations are not interchangeable in this temperature range. In the $^{13}C\{^1H\}$ and (to some extent) ^1H NMR spectra, all positions of the 16-TMC ligand have been assigned and the peak(s) listed for each position correspond to signal(s) of greater intensity (see Supporting Information for spectra of **6**). Fast atom bombardment (FAB) mass spectra were obtained on a Finnigan MAT 95 mass spectrometer with a 3-nitrobenzyl alcohol matrix. Infrared spectra were recorded as KBr plates on a Bio-Rad FT-IR spectrometer. UV−vis spectra were recorded on a Perkin-Elmer Lambda 19 spectrophotometer. Elemental analyses were performed by the Institute of Chemistry, Chinese Academy of Sciences, Beijing.

Cyclic voltammetry was performed with a Princeton Applied Research Model 273A potentiostat. A conventional two-compartment electrochemical cell was used. The glassy-carbon electrode was polished with 0.05 μm alumina on a microcloth, sonicated for 5 min in deionized water, and rinsed with acetonitrile before use. An $Ag/AgNO_3$ (0.1 M in CH_3CN) electrode was used as reference electrode. All solutions were degassed with argon before experiments. $E_{1/2}$ values are the average of the cathodic and anodic peak potentials for the oxidative and reductive waves. The $E_{1/2}$ value of the ferrocenium/ferrocene couple ($Cp_2Fe^{+/0}$) measured in the same solution was used as an internal reference, and all reported $E_{1/2}$ values are referenced to the $Cp_2Fe^{+/0}$ couple.

Resonance Raman Spectroscopy. The resonance Raman apparatus and methods have previously been described in detail,[18] and a summary is given here. The first anti-Stokes Raman-shifted line of the second harmonic of an Nd:YAG laser provided the excitation frequency for the resonance Raman experiment. The laser beam was loosely focused onto the sample using ∼130° backscattering geometry, and reflective optics were used to collect the Raman-scattered light and image it through a depolarizer and entrance slit of a 0.5 m spectrograph equipped with a 1200 groove/mm ruled grating blazed at 250 nm. The light was dispersed onto a liquid nitrogen cooled CCD detector. Accumulations of about 1 min were acquired from the CCD, and about 30 of these scans were added to afford the resonance Raman spectrum. Known acetonitrile solvent bands were used to calibrate the Raman shifts of the resonance Raman spectrum. Appropriately scaled solvent and quartz cell background spectra (accumulated simultaneously with the sample spectra on a different part of the CCD) were subtracted to remove the solvent bands, the Rayleigh line, and the quartz cell background signal from the resonance Raman spectrum.

Computational Methodology. The ab initio calculations were performed on the model complex $[Cl(NH_3)_4Ru=C=C=CPh_2]^+$ (with C_1 symmetry), which was used as a computational model for $[Cl(16\text{-}TMC)Ru=C=C=CAr_2]^+$ (**6**−**9**). The geometry of the complex was optimized at second-order Møller−Plesset (MP2) level. The large orbital basis sets with relativistic effective core potential CRENBL ECP proposed by Christiansen et al.[19] were employed, i.e., H (4s), C, N, Cl (ECP, 4s, 4p), and Ru (ECP, 5s, 5p, 4d), and the number of valence electrons involved for Ru, C, N, and Cl were 16, 4, 5, and 7, respectively. Therefore, the calculations employed 448 basis functions and 124 electrons. The natural charges were calculated using natural population analysis.[20] The calculations were accomplished using the Gaussian 98 program[21] on a PC, natural population analysis was performed using NBO version 3.1[22] distributed in Gaussian 98, and the molecular graphics are presented using MOLEKEL version 4.3.[23]

Synthesis. $[Cl(16\text{-}TMC)Ru=C=CH(C_6H_4X\text{-}4)]PF_6$ (1−4). Excess $HC\equiv CC_6H_4X$-4 (1 mmol) was added to a mixture containing $[Ru(16\text{-}TMC)Cl_2]Cl$ (0.10 g, 0.20 mmol) and zinc amalgam in methanol (30 mL). After refluxing for 2 h, the resultant green solution was filtered and added to a saturated methanolic solution of NH_4PF_6 to afford a green crystalline solid. This solid was recrystallized by slow diffusion of Et_2O into a CH_2Cl_2 solution to give bright green crystals. Complex **1** (X = H): yield 0.09 g, 67%. Anal. Calcd for $C_{24}H_{42}N_4RuClPF_6$: C, 43.15; H, 6.34; N, 8.39. Found: C, 42.99; H, 6.36; N, 8.28. ^1H NMR (500 MHz, $(CD_3)_2CO$): δ 1.50−1.58, 1.86−2.26 (m, 16H, CH_2), 2.47, 2.70, 2.73 (singlets, 12H, NCH_3), 3.29−4.13 (m, 8H, CH_2), 4.83, 4.89 (2 × s, 1H, =CH), 7.16−7.55 (m, 5H, C_6H_5). $^{13}C\{^1H\}$ NMR (126 MHz, $(CD_3)_2CO$): δ 20.9, 21.0 (NCH_2CH_2); 45.0, 48.1, 50.5, 51.3, 55.2 (NCH_3); 57.8, 58.1, 61.1, 62.4, 65.7, 66.1, 67.2, 68.6 (NCH_2); 111.1, 111.4 (C_β); 126.5, 126.6, 128.5, 128.6, 129.2 (aryl C); 127.4, 127.7 (C_{ipso}); 349.4, 351.5 (C_α). IR (cm^{-1}): $\nu_{C=C}$ = 1593, 1607, ν_{P-F} = 834. FAB-MS: *m*/*z* 523 [M^+]. See Supporting Information for **2**−**4**.

$[Cl(16\text{-}TMC)Ru=C=CHCHPh_2]PF_6$ (5). The procedure for **1**−**4** was adopted, but 1,1-diphenyl-2-propyn-1-ol was used instead of the acetylene substrate. Addition of a saturated methanolic solution of NH_4PF_6 afforded a pale red crystalline solid, which was recrystallized from CH_2Cl_2/Et_2O to give bright red crystals. Yield 0.11 g, 73%. Anal. Calcd for $C_{31}H_{48}N_4RuClPF_6$: C, 49.11; H, 6.38; N, 7.39. Found: C, 48.99; H, 6.41; N, 7.44. ^1H NMR (500 MHz, $(CD_3)_2CO$): δ 1.46−1.52, 1.80−

(14) Katayama, H.; Ozawa, F. *Organometallics* **1998**, *17*, 5190−5196.
(15) Touchard, D.; Pirio, N.; Dixneuf, P. H. *Organometallics* **1995**, *14*, 4920−4928.
(16) Sullivan, B. P.; Meyer, T. J. *Inorg. Chem.* **1982**, *21*, 1037−1040.
(17) (a) Che, C.-M.; Cheng, W.-K.; Lai, T.-F.; Poon, C.-K.; Mak, T. C. W. *Inorg. Chem.* **1987**, *26*, 1678−1683. (b) Che, C.-M.; Wong, K.-Y.; Mak, T. C. W. *Chem. Commun.* **1985**, 988−990. (c) Mak, T. C. W.; Che, C.-M.; Wong, K.-Y. *Chem. Commun.* **1985**, 986−988. (d) Che, C.-M.; Wong, K.-Y.; Mak, T. C. W. *Chem. Commun.* **1985**, 546−548.
(18) Zheng, X.; Phillips, D. L. *J. Chem. Phys.* **1998**, *108*, 5772−5783.
(19) (a) Pacios, L. F.; Christiansen, P. A. *J. Chem. Phys.* **1985**, *82*, 2664−2671. (b) LaJohn, L. A.; Christiansen, P. A.; Ross, R. B.; Atashroo, T.; Ermler, W. C. *J. Chem. Phys.* **1987**, *87*, 2812−2824. Basis sets were obtained from the Extensible Computational Chemistry Environment Basis Set Database, Version 6/19/03, as developed and distributed by the Molecular Science Computing Facility, Environmental and Molecular Sciences Laboratory which is part of the Pacific Northwest Laboratory, P.O. Box 999, Richland, WA 99352 and funded by the U.S. Department of Energy. The Pacific Northwest Laboratory is a multiprogram laboratory operated by Battelle Memorial Institute for the U.S. Department of Energy under contract DE-AC06-76RLO 1830. Contact David Feller or Karen Schuchardt for further information.
(20) (a) Reed, A. E.; Weinstock, R. B.; Weinhold, F. *J. Chem. Phys.* **1985**, *83*, 735−746. (b) Reed, A. E.; Weinhold, F. *J. Chem. Phys.* **1983**, *78*, 4066−4073.
(21) Frisch, M. J.; Trucks, G. W.; Schlegel, H. B.; Scuseria, G. E.; Robb, M. A.; Cheeseman, J. R.; Zakrzewski, V. G.; Montgomery, J. A., Jr.; Stratmann, R. E.; Burant, J. C.; Dapprich, S.; Millam, J. M.; Daniels, A. D.; Kudin, K. N.; Strain, M. C.; Farkas, O.; Tomasi, J.; Barone, V.; Cossi, M.; Cammi, R.; Mennucci, B.; Pomelli, C.; Adamo, C.; Clifford, S.; Ochterski, J.; Petersson, G. A.; Ayala, P. Y.; Cui, Q.; Morokuma, K.; Malick, D. K.; Rabuck, A. D.; Raghavachari, K.; Foresman, J. B.; Cioslowski, J.; Ortiz, J. V.; Baboul, A. G.; Stefanov, B. B.; Liu, G.; Liashenko, A.; Piskorz, P.; Komaromi, I.; Gomperts, R.; Martin, R. L.; Fox, D. J.; Keith, T.; Al-Laham, M. A.; Peng, C. Y.; Nanayakkara, A.; Gonzalez, C.; Challacombe, M.; Gill, P. M. W.; Johnson, B. G.; Chen, W.; Wong, M. W.; Andres, J. L.; Head-Gordon, M.; Replogle, E. S.; Pople, J. A. *Gaussian 98* (Revision A.7); Gaussian, Inc.: Pittsburgh, PA, 1998.
(22) Glendening, E. D.; Reed, A. E.; Carpenter, J. E.; Weinhold, F. *NBO 3.1*. Board of Regents of the University of Wisconsin System on behalf of the Theoretical Chemistry Institute, 1996−2003.
(23) (a) Flukiger, P.; Luthi, H. P.; Portmann, S.; Weber, J. *MOLEKEL 4.3*; Swiss Center for Scientific Computing: Manno, Switzerland, 2000−2002. (b) Portmann, S.; Luthi, H. P. *Chimia* **2000**, *54*, 766−770.

2.28 (m, 16H, CH_2), 2.42, 2.58, 2.61 (singlets, 12H, NCH_3), 3.18−4.06 (m, 8H, CH_2), 4.68, 4.74 (2 × d, 1H, $^3J_{HH}$ = 10.5 Hz, =CH,), 6.01, 6.03 (2 × d, 1H, $^3J_{HH}$ = 10.5 Hz, $CHPh_2$), 7.23−7.60 (m, 10H, C_6H_5). $^{13}C\{^1H\}$ NMR (126 MHz, $(CD_3)_2CO$): δ 20.9, 21.6 (NCH_2CH_2); 42.1, 42.4 ($CHPh_2$); 44.8, 48.0, 50.4, 50.8, 54.8 (NCH_3); 57.5, 57.9, 61.0, 62.4, 65.7, 66.0, 67.1, 69.4 (NCH_2); 112.1, 112.4 (C_β); 126.8, 128.0, 128.9 (aryl C); 145.9, 146.0 (C_{ipso}); 347.4, 350.5 (C_α). IR (cm^{-1}): $\nu_{C=C}$ = 1631, ν_{P-F} = 839. FAB-MS: *m*/*z* 613 [M^+].

[Cl(16-TMC)Ru=C=C=C(C$_6$H$_4$X-4)$_2$]PF$_6$ (6−9). A methanolic solution (30 mL) of [Ru(16-TMC)Cl_2]Cl (0.10 g, 0.20 mmol) was refluxed in the presence of zinc amalgam for 10 min. This was filtered to give a green solution, and excess HC≡CC(C_6H_4X-4)$_2$OH (0.40 mol) was then added. After refluxing for 2 h, the resultant deep red solution was filtered and added to a saturated methanolic solution of NH_4PF_6 to afford a red crystalline solid. The crude red solid was dissolved in a minimum amount of CH_2Cl_2, and slow diffusion of Et_2O into this solution afforded deep red crystals. Complex **6** (X = H): yield 0.11 g, 73%. Anal. Calcd for $C_{31}H_{46}N_4RuClPF_6$: C, 49.24; H, 6.13; N, 7.41. Found: C, 49.29; H, 6.20; N, 7.65. ^1H NMR (500 MHz, $(CD_3)_2CO$): δ 1.38−1.48, 1.67−2.28 (m, 16H, CH_2), 2.36, 2.39, 2.52 (singlets, 12H, NCH_3), 3.05−4.04 (m, 8H, CH_2), 7.35−7.48 (m, 4H, H_o), 7.85−7.91 (m, 2H, H_p), 8.07−8.11 (m, 4H, H_m). $^{13}C\{^1H\}$ NMR (126 MHz, $(CD_3)_2$-CO): δ 20.9, 21.6 (NCH_2CH_2); 44.6, 48.1, 50.6, 50.7, 54.4 (NCH_3); 57.6, 57.8, 58.0, 61.3, 61.7, 65.9, 66.2, 67.0, 69.9 (NCH_2); 127.1, 129.7, 130.0 (aryl C); 150.1, 150.7 (C_γ); 150.9, 151.0 (C_{ipso}); 248.7, 250.7 (C_β); 302.9, 308.6 (C_α). IR (cm^{-1}): $\nu_{C=C=C}$ = 1884, ν_{P-F} = 841. FAB-MS: *m*/*z* 611 [M^+]. See Supporting Information for **7**−**9**.

[Cl(dppm)$_2$Os=C=C=C(C$_6$H$_4$X-4)$_2$]PF$_6$ (13−15). To a CH_2Cl_2 solution (30 mL) of HC≡CC(C_6H_4X-4)$_2$OH (0.50 mol) and $NaPF_6$ (0.1 g, 0.60 mmol) was added *cis*-[Os(dppm)$_2Cl_2$] (0.15 g, 0.27 mmol). After stirring for 3 h at room temperature, the color of the solution turned deep violet then deep orange-red. The reaction mixture was stirred for an additional 12 h and filtered. All volatile components were removed under vacuum. The resultant red solid was washed with Et_2O (3 × 15 mL) and recrystallized by slow diffusion of Et_2O into a CH_2Cl_2 solution to give bright red crystals. Complex **13** (X = H): yield 0.25 g, 75%. Anal. Calcd for $C_{65}H_{54}OsClP_5F_6$: C, 58.72; H, 4.09. Found: C, 58.81; H, 4.03. ^1H NMR (400 MHz, $(CD_3)_2CO$): δ 5.99−6.25 (m, 4H, PCH_2P), 6.69−7.78 (m, 50H, aryl H). $^{13}C\{^1H\}$ NMR (100 MHz, $(CD_3)_2$-CO): δ 50.6 (PCH_2P), 128.0−133.3 (aryl C), 150.3 (C_{ipso}), 155.4 (C_γ), 225.6 (C_β), 270.8 (C_α). $^{31}P\{^1H\}$ NMR (162 MHz, $(CD_3)_2CO$): δ −57.7 (s), −144.1 (sept, PF_6, $^1J_{PF}$ = 708 Hz). IR (cm^{-1}): $\nu_{C=C=C}$ = 1924, ν_{P-F} = 839. FAB-MS: *m*/*z* 1183 [M^+]. See Supporting Information for **14** and **15**.

X-ray Crystallography. The crystal data and details of data collection and refinement for **1**·CH_2Cl_2, **5**·CH_2Cl_2, **6**, and **8** are summarized in Table S1 (see Supporting Information). A MAR diffractometer with a 300 mm image plate detector using graphite-monochromatized Mo Kα radiation (λ = 0.71073 Å) was employed for data collection. The images were interpreted and intensities integrated using program DENZO,[24] and structures were solved by direct methods employing the SIR-97 program[25] on a PC. The Ru, Cl, and many non-H atoms were located according to the direct methods. The positions of the other non-hydrogen atoms were found after successful refinement by full-matrix least-squares using program SHELXL-97 on PC.[26] Except for disordered atoms, non-hydrogen atoms were refined anisotropically in the final stage of least-squares refinement. Unless otherwise stated, the positions of H atoms were calculated based on riding mode with thermal parameters equal to 1.2 times that of the associated C atom. For **1**·CH_2Cl_2, two formula units were located in the asymmetric unit. Disorder is observed in the $(CH_2)_3$ units of the 16-TMC ligands, and some restraints had been applied. In the final stage of least-squares refinement, the disordered atoms and C(50) of the solvent molecule were refined isotropically. For **5**·CH_2Cl_2, one crystallographic asymmetric unit consists of one formula unit. The CH_3 and two CH_2 groups bound to N(3) in the 16-TMC ligand, plus the PF_6^- unit, are disordered. For **6**, one crystallographic asymmetric unit consists of one formula unit. Disorder was found concerning groups bound to N(3) and N(4), which were refined isotropically. For **8**, one crystallographic asymmetric unit consists of one-half of one formula unit. The $(CH_2)_3$ groups of the 16-TMC ligand are disordered, and restraints have been applied.

Scheme 1

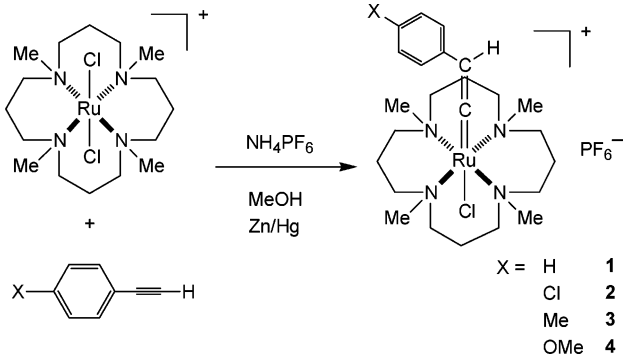

Results

Synthesis and Characterization. In the literature, extensive studies on the preparation of vinylidene− and allenylidene−ruthenium complexes [formulated as Ru(II)] supported by phosphine and arene ligands have appeared.[3] In the present work, we synthesized ruthenium derivatives containing the macrocyclic amine ligand 16-TMC. Unlike other literature methods, a Ru(III) rather than Ru(II) precursor was used because the Ru(II) species [Ru(16-TMC)Cl_2] cannot be isolated. The in situ reduction of [Ru(16-TMC)Cl_2]Cl by zinc amalgam resulted in the generation of a Ru(II) species, the chloride ligands of which are more reactive to substitution.[27] Hence, reaction of [Ru(16-TMC)Cl_2]Cl and HC≡CR in the presence of zinc amalgam in refluxing methanol afforded the vinylidene−ruthenium complexes **1**−**4** (Scheme 1) with an overall yield of around 70% (for synthesis of the related derivative **5**, see below). Slow diffusion of Et_2O into a CH_2Cl_2 solution under inert-atmosphere conditions yielded analytically pure crystalline solids. The vinylidene complexes are mildly unstable upon exposure to air in both solid and solution forms; oxidative cleavage of the vinylidene ligands occurs within 10 h in solution to give a carbonyl complex (characterized by its $\nu_{C\equiv O}$ at 1917 cm^{-1}).

No reaction was observed between **1**−**5** and methanol upon refluxing for 48 h, although there have been reports of vinylidene−ruthenium complexes that react with methanol to give methoxyalkylcarbene complexes.[1b,3m] Their resistance to attack by methanol is presumably a result of both steric and electronic factors; the four NMe groups of 16-TMC may provide protection for the C_α atom, while the 16-TMC ligand is a pure σ-donor that increases the π-basicity of the ruthenium ion, making C_α less susceptible to nucleophilic attack. By monitoring the vinylidene proton signal of complex **1** by ^1H NMR

(24) DENZO: In *The HKL Manual−A description of programs DENZO, XDISPLAYF and SCALEPACK*; written by Gewirth, D. with the cooperation of the program authors Otwinowski, Z.; Minor, W.; Yale University: New Haven, CT, 1995.
(25) SIR-97: Altomare, A.; Burla, M. C.; Camalli, M.; Cascarano, G.; Giacovazzo, C.; Guagliardi, A.; Moliterni, A. G. G.; Polidori, G.; Spagna, R. *J. Appl. Crystallogr.* **1998**, *32*, 115−119.
(26) SHELXL-97: Sheldrick, G. M. Programs for Crystal Structure Analysis (release 97−2); University of Goetingen: Germany, 1997.
(27) Poon, C.-K.; Che, C.-M.; Kan, Y.-P. *J. Chem. Soc., Dalton Trans.* **1980**, 128−133.

Scheme 2

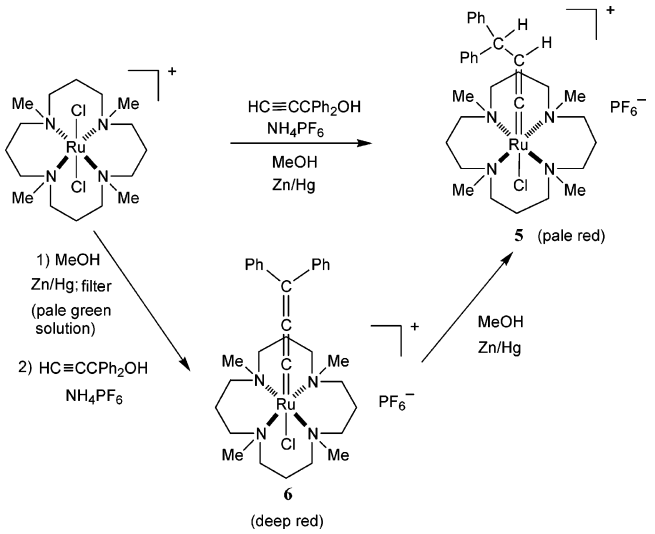

Scheme 3

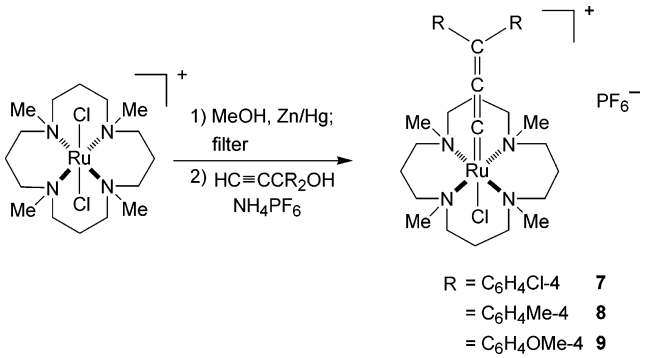

spectroscopy, deprotonation of the vinylidene ligand was achieved upon addition of sodium methoxide but not triethylamine. This is in contrast to the reactivity of phosphine-supported analogues such as *trans*-[Cl(dppe)$_2$Ru=C=CHR]PF$_6$ and *trans*-[Cl(dppm)$_2$Ru=C=CHR]PF$_6$, which have been observed to interact with triethylamine to give the corresponding acetylide complexes.[28]

The vinylidene complexes have been characterized by various spectroscopic techniques. The ^{1}H signals at 4.83−4.91 ppm,[29] together with typical low-field ^{13}C NMR signals at 347.4−353.1 ppm, confirm the presence of the vinylidene moiety. The IR spectra also show $\nu_{C=C}$ stretching frequencies at 1593−1631 cm^{-1}, which are among the lowest reported for vinylidene−ruthenium derivatives.[1b] For example, the $\nu_{C=C}$ values (1593 and 1607 cm^{-1}) for *trans*-[Cl(16-TMC)Ru=C=CHPh]PF$_6$ (**1**) are noticeably lower than that of 1628 cm^{-1} for *trans*-[Cl(dppe)$_2$Ru=C=CHPh]PF$_6$ and 1658 cm^{-1} for *trans*-[Cl(dppm)$_2$Ru=C=CHPh]PF$_6$.[28]

Preparation of allenylidene derivatives were attempted using propargylic alcohols following the synthetic strategy depicted at the top of Scheme 2. Upon refluxing a mixture of 1,1-diphenyl-2-propyn-1-ol and [Ru(16-TMC)Cl$_2$]Cl in the presence of zinc amalgam in methanol, a pale red solid was isolated that exhibits an IR band at 1631 cm^{-1}. Its mass spectrum revealed a parent molecular ion peak at 613, and the ^{1}H NMR spectrum contained a vinylidene proton (4.68, 4.74 ppm) that is coupled to another deshielded proton (6.01, 6.03 ppm, J_{HH} = 10.5 Hz). This complex was formulated as the vinylidene derivative [Cl(16-TMC)Ru=C=CH−CHPh$_2$]PF$_6$ (**5**), and the molecular structure was confirmed by X-ray crystal analysis (see below).

We suspected that the presence of the zinc amalgam reagent throughout the reaction caused the formation of complex **5**. Therefore, the synthetic methodology was modified and performed in sequence (see bottom of Scheme 2). [Ru(16-TMC)Cl$_2$]Cl was first reduced to a Ru(II) species by zinc amalgam in methanol. The resultant pale green solution was then filtered and refluxed with 1,1-diphenyl-2-propyn-1-ol in the absence of zinc amalgam. A deep red product was isolated and found to exhibit an intense IR stretching band at 1884 cm^{-1}, which is comparable to reported $\nu_{C=C=C}$ values for ruthenium−allenylidene complexes.[1a] On the basis of FAB-MS and ^{1}H and ^{13}C NMR data, the deep red product was identified as [Cl(16-TMC)Ru=C=C=CPh$_2$]PF$_6$ (**6**). This synthetic route was therefore employed to synthesize the substituted allenylidene derivatives **7**−**9** (Scheme 3).

Our observations suggest that the vinylidene complex **5** was formed via the allenylidene derivative **6** (its deep red color was observed en route to the generation of **5**), and this is strongly supported by the fact that **6** can be converted to **5** upon refluxing in methanol in the presence of Zn/Hg. It is interesting to note that the apparent hydrogen-atom addition process only occurs at C$_\beta$/C$_\gamma$ but not C$_\alpha$/C$_\beta$, plus this reaction does not ensue for the vinylidene complexes.

Although there have been accounts of allenylidene−ruthenium complexes which react with methanol to give unsaturated carbene derivatives, no reaction was observed between **6**−**9** and methanol upon refluxing for 48 h. In addition, complex **6** remained intact after treatment with NaOMe (20 equiv) in methanol for 48 h at room temperature. In contrast, the diphosphine analogues *trans*-[Cl(dppm)$_2$Ru=C=C=CR$_2$]PF$_6$ react with NaOMe to give *trans*-[Cl(dppm)$_2$Ru−C≡C−C(OMe)-R$_2$] derivatives.[15] Also, no reaction was detected between complex **6** and 100 equiv of CF$_3$COOH in CH$_2$Cl$_2$ after 10 h.

Complexes **6**−**9** display low-field ^{13}C NMR signals for C$_\alpha$ (294.6−308.6 ppm), C$_\beta$ (229.1−257.3 ppm), and C$_\gamma$ (149.1−150.7 ppm). Like the vinylidene complexes, the $\nu_{C=C=C}$ in this work are among the lowest reported for allenylidene−ruthenium derivatives. For example, the $\nu_{C=C=C}$ for **6** appears at 1884 cm^{-1}, while for the phosphine-supported congeners *trans*-[Cl(dppm)$_2$-Ru=C=C=CPh$_2$]PF$_6$ (**10**) and *trans*-[Cl(dppe)$_2$Ru=C=C=CPh$_2$]PF$_6$, $\nu_{C=C=C}$ is observed at 1928 and 1923 cm^{-1} respectively.[15,30]

It was found that the reaction of [Ru(16-TMC)Cl$_2$]$^+$ with 1-phenyl-2-propyn-1-ol according to Scheme 3 did not cleanly yield an allenylidene complex. When the reaction was carried out in methanol, a mixture of [Cl(16-TMC)Ru=C=CH−CH(OMe)Ph]PF$_6$ ($\nu_{C=C}$ = 1608 cm^{-1}; ^{1}H NMR: 3.35 (OMe), 4.12, 4.17 (=C=CH), 6.10, 6.13 ppm (=C=CH−C*H*), $^3J_{HH}$ = 8.2 Hz; M$^+$ = 567) and [Cl(16-TMC)Ru=C=C=CHPh]PF$_6$ ($\nu_{C=C}$ = 1887 cm^{-1}; ^{1}H NMR: 8.35, 8.37 ppm (=C=C=CH);

(28) (a) Touchard, D.; Haquette, P.; Guesmi, S.; Pichon, L. L.; Daridor, A.; Toupet, L.; Dixneuf, P. H. *Organometallics* **1997**, *16*, 3640−3648. (b) Touchard, D.; Haquette, P.; Pirio, N.; Toupet, L.; Dixneuf, P. H. *Organometallics* **1993**, *12*, 3132−3139.

(29) Two singlets are observed for the vinylidene proton in the ^{1}H NMR spectra of **1**−**4** due to the existence of two prevalent conformations for the 16-TMC ligand in solution (see Experimental Section and Supporting Information).

(30) Touchard, D.; Guesmi, S.; Bouchaib, M.; Haquette, P.; Daridor, A.; Dixneuf, P. H. *Organometallics* **1996**, *15*, 2579−2581.

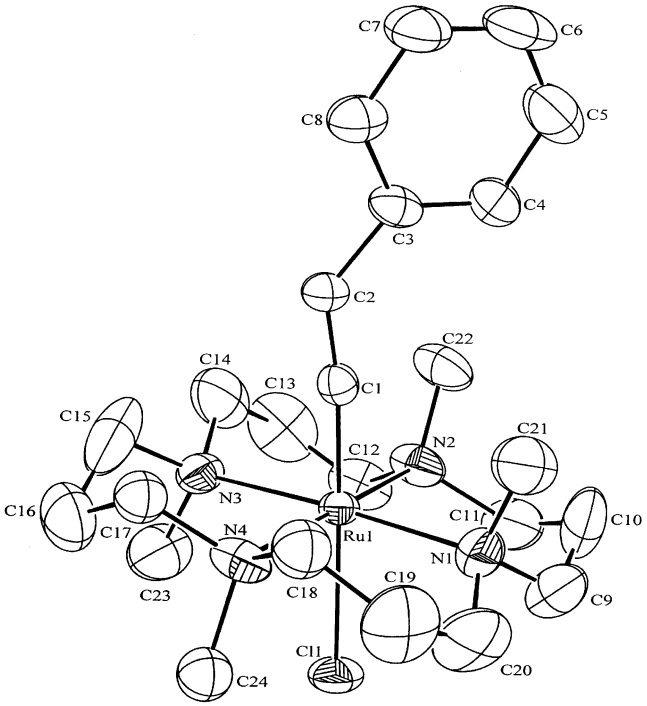

Figure 1. Perspective view of one of the two cations in **1** (30% probability ellipsoids).

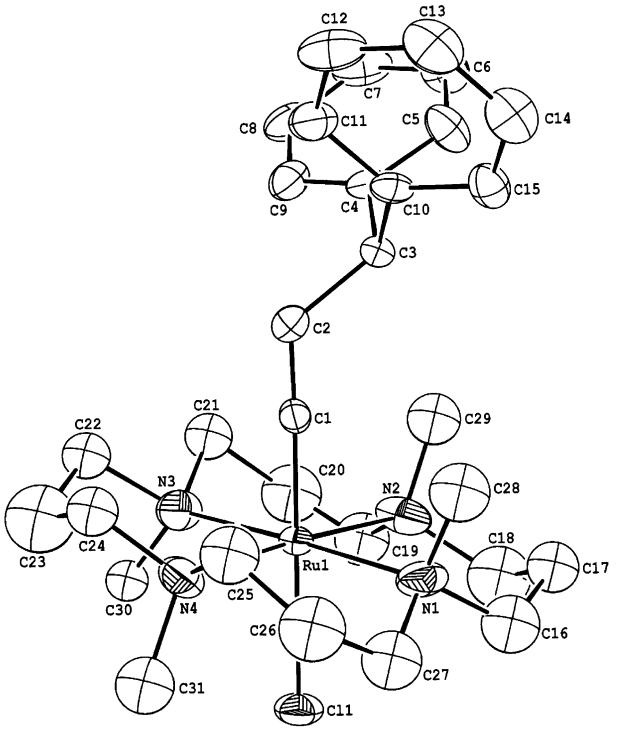

Figure 2. Perspective view of the cation in **5** (30% probability ellipsoids).

Scheme 4

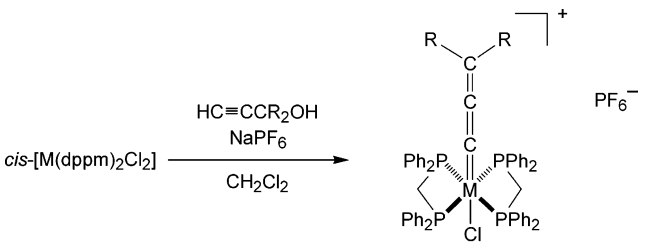

M = Ru	R = C_6H_5	**10**	M = Os	R = C_6H_5	**13**
	= C_6H_4Cl-4	**11**		= C_6H_4Cl-4	**14**
	= C_6H_4Me-4	**12**		= C_6H_4Me-4	**15**

$M^+ = 534$) was obtained. If CH_2Cl_2 was used as solvent, both [Cl(16-TMC)Ru═C═CH−CH(OH)Ph]PF_6 and the desired complex [Cl(16-TMC)Ru═C═C═CHPh]PF_6 were isolated.

Allenylidene−ruthenium[15] and −osmium complexes supported by the bidentate phosphine ligand dppm (bis(diphenylphosphino)methane) were prepared according to Scheme 4. Reaction of *cis*-[$M(dppm)_2Cl_2$] and propargylic alcohols in the presence of $NaPF_6$ in CH_2Cl_2 gave *trans*-[$Cl(dppm)_2M$═C═C═CR_2]PF_6 (M = Ru, **10**−**12**; M = Os, **13**−**15**). The osmium derivatives **13**−**15** also display low-field ^{13}C NMR signals for C_α (266.9−271.0 ppm), C_β (218.2−231.3 ppm), and C_γ (150.7−156.3 ppm). It is interesting to note that the $\nu_{C=C=C}$ for **13**−**15** are comparable to the ruthenium analogues. For example, the $\nu_{C=C=C}$ for *trans*-[$Cl(dppm)_2M$═C═C═CPh_2]PF_6 appears at 1924 and 1928 cm^{-1} for M = Os (**13**) and Ru (**10**),[15] respectively.

Crystal Structures. The molecular structures of **1**, **5**, **6**, and **8** have been determined by X-ray crystallography. Perspective views of the complex cations of **1**, **5**, and **6** are shown in Figures 1, 2, and 3, respectively. Relevant bond lengths and angles are listed in Table 1. In each case, the Ru atom resides in a distorted octahedral environment comprising the four nitrogen atoms of

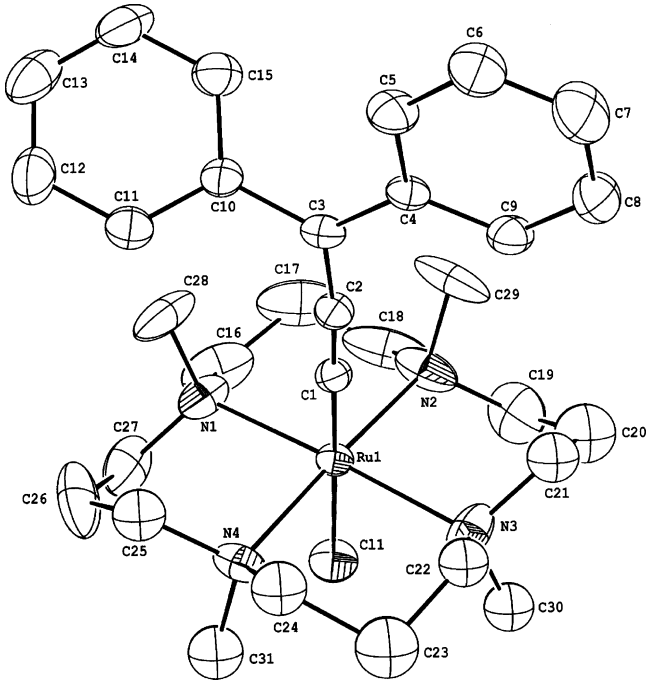

Figure 3. Perspective view of the cation in **6** (30% probability ellipsoids).

16-TMC plus the chloro and vinylidene or allenylidene ligands that are trans to each other. The disorder of the 16-TMC moiety in these structures demonstrate that several conformations can exist upon coordination to the Ru center,[12b,17] and those where the four *N*-methyl groups adopt the 'two up, two down' and 'three up, one down' configurations are prevalent. The Ru(1)−C(1)−C(2) angle for the vinylidene and allenylidene complexes approach linearity. The Ru(1)−C(1) [1.780(8)−1.862(7) Å], C(1)−C(2) [1.239(10)−1.352(10) Å], and C(2)−C(3) distances [**6**, 1.339(7) Å; **8**, 1.378(10) Å] and C(1)−C(2)−C(3) angles [**6**, 170.1(5)°; **8**, 180°] are comparable to those for analogous

Table 1. Selected Bond Length (Å) and Angles (deg)

	1	**5**	**6**	**8**
Ru−C(1)	1.780(8)	1.802(7)	1.849(4)	1.862(7)
C(1)−C(2)	1.352(10)	1.309(10)	1.262(7)	1.24(1)
C(2)−C(3)	1.474(11)	1.523(10)	1.339(7)	1.378(10)
Ru−Cl(1)	2.488(2)	2.489(2)	2.478(1)	2.449(2)
Ru−C(1)−C(2)	172.6(7)	177.8(6)	177.6(4)	180
Cl−Ru−C(1)	178.4(2)	179.7(2)	178.0(2)	180
C(1)−C(2)−C(3)	134.2(8)	126.2(7)	170.1(5)	180
mean Ru−N	2.253	2.247	2.258	2.260

Table 2. Electrochemical Data for *trans*-[Cl(16-TMC)Ru=C=CH−CHPh$_2$]PF$_6$ (**5**), *trans*-[Cl(16-TMC)Ru=C=C=C(C$_6$H$_4$X-4)$_2$]PF$_6$ (**6**−**9**), and *trans*-[Cl(dppm)$_2$M=C=C=C(C$_6$H$_4$X-4)$_2$]PF$_6$ (M = Ru, **10**−**12**; M = Os, **13**−**15**)[a]

complex	$E_{1/2}$/ V vs $Cp_2Fe^{+/0}$	
5	0.81[b]	−2.16[c]
6 (X = H)	0.64	−1.27
7 (X = Cl)	0.70	−1.19
8 (X = Me)	0.57	−1.32
9 (X = OMe)	0.49	−1.42
10 (X = H)	1.02	−0.98
11 (X = Cl)	1.06	−0.92
12 (X = Me)	0.92	−1.02
13 (X = H)	0.82	−1.14
14 (X = Cl)	0.88	−1.05
15 (X = Me)	0.75	−1.20

[a] Supporting electrolyte: 0.1 M [^{n}Bu$_4$N]PF$_6$ in CH$_3$CN. The potential $E_{1/2} = (E_{pc} + E_{pa})/2$ at 25 °C for reversible couples. [b] Irreversible; the recorded potential is the anodic peak potential at a scan rate of 50 mV s^{-1}. [c] Irreversible; the recorded potential is the cathodic peak potential at a scan rate of 50 mV s^{-1}.

complexes in the literature[1] [vinylidene: Ru−C(1) = 1.76−1.91 Å, C(1)−C(2) = 1.14−1.34 Å; allenylidene: Ru−C(1) = 1.84−2.00 Å, C(1)−C(2) = 1.18−1.27 Å, C(2)−C(3) = 1.35−1.41 Å]. For **5**, the angles around the C(3) atom are consistent with sp^3 hybridization. The molecular structures show that the C$_\alpha$ atoms of the vinylidene/allenylidene ligands are shielded by the NMe groups of the 16-TMC ligand. The Ru−C$_\alpha$ distances in the allenylidene complexes **6** and **8** are slightly longer than those in **1** and **5**, and the C$_\alpha$−C$_\beta$ bonds for **6** and **8** are significantly shorter. The Ru−C$_\alpha$ and C$_\alpha$−C$_\beta$ bond lengths in **6** and **8** are thus intermediate compared to those of vinylidene and acetylide relatives (for *trans*-[Ru(16-TMC)(C≡CPh)$_2$],[11b] Ru−C$_\alpha$ = 2.077(4) Å, C$_\alpha$−C$_\beta$ = 1.198(6) Å).

Electrochemistry. Cyclic voltammetry was used to examine the electrochemistry of the vinylidene−ruthenium complex **5** and the allenylidene−ruthenium (**6**−**12**) and −osmium (**13**−**15**) complexes. The electrochemical data are listed in Table 2, and the cyclic voltammograms of **6**, **10**, and **13** are depicted in Figure 4. Complex **5** gives two irreversible couples at −2.16 and 0.81 V vs $Cp_2Fe^{+/0}$. The cyclic voltammograms of complexes **6**−**9** contain two reversible couples, namely, a reduction wave at $E_{1/2}$ = −1.42 to −1.19 V and an oxidation wave at $E_{1/2}$ = 0.49 to 0.70 V. The $E_{1/2}$ value of each couple decreases with an increase in the electron-donating capacity of the C$_6$H$_4$X-4 substituents [0.70, −1.19 V for **7** (X = Cl); 0.64, −1.27 V for **6** (X = H); 0.57, −1.32 V for **8** (X = Me); 0.49, −1.42 V for **9** (X = OMe)]. The change in the $E_{1/2}$ values from X = Cl to OMe is around 200 mV for each couple. Complexes **10**−**12** and **13**−**15** also show two reversible couples, and similar trends in $E_{1/2}$ values are observed [1.06, −0.92 V for **11** (X = Cl); 1.02, −0.98 V for **10** (X = H); 0.92, −1.02 V for **12** (X = Me); 0.88, −1.05 V for **14** (X = Cl); 0.82, −1.14 V for **13** (X = H); 0.75, −1.20 V for **15** (X = Me)]. The $E_{1/2}$ values for the two waves of **10**−**12** are around 270−380 mV more anodic than those of the 16-TMC analogues **6**−**8**. In the literature, a reduction couple was reported for *trans*-[Cl(dppe)$_2$-Ru=C=C=C(C$_6$H$_4$X-4)$_2$]PF$_6$ with a comparable trend for the shift in $E_{1/2}$ values [−0.97, −1.05, −1.06, and −1.24 V for X = Cl, F, H, and OMe, respectively].[3k] Recently, Dixneuf and co-workers reported two redox couples for [Cl(dppe)$_2$Ru=C=C=CPh$_2$]PF$_6$ (E_{ox} = 0.99 and E_{red} = −1.03 V),[3b] which are 350 and 240 mV more anodic than the corresponding values for **6,** respectively.

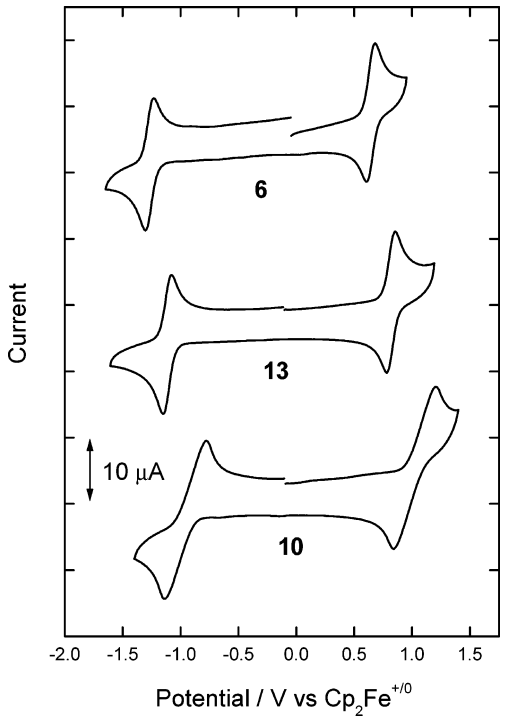

Figure 4. Cyclic voltammograms for [Cl(16-TMC)Ru=C=C=CPh$_2$]PF$_6$ (**6**) and [Cl(dppm)$_2$M=C=C=CPh$_2$]PF$_6$ [M = Ru (**10**) and Os (**13**)] in CH$_3$CN with [^{n}Bu$_4$N]PF$_6$ (0.1 M) as supporting electrolyte. Conditions: working electrode, glassy-carbon; scan rate, 50 mV s^{-1}.

Electronic Spectroscopy. The UV−vis absorption data of complexes **1**−**15** (in CH$_3$CN) and RuCl$_2${(=C)$_n$HPh}(PCy$_3$)$_2$ (n = 1 and 2; in CH$_2$Cl$_2$) are summarized in Table 3. The absorption spectra of **2**, **4**, **5**, and RuCl$_2${(=C)$_n$HPh}(PCy$_3$)$_2$ (n = 1 and 2) are depicted in Figure 5. For the vinylidene complexes, the intense high-energy bands at $\lambda_{max} \leq 310$ nm ($\epsilon_{max} \geq 10^4$ dm^3 mol^{-1} cm^{-1}) for **1**−**4** are similar, but they are distinct from that of **5** where the Ru=C=C and phenyl moieties are separated by a saturated carbon atom. Nevertheless, complexes **1**−**5** all exhibit weak low-energy bands at λ_{max} = 460−640 nm with ϵ values below 10^2 dm^3 mol^{-1} cm^{-1}. The spectrum of RuCl$_2$(=C=CHPh)(PCy$_3$)$_2$ is similar to those of the vinylidene complexes **1**−**4**. It is interesting to note that the UV−vis absorption spectrum of the Grubbs catalyst RuCl$_2$-(=CHPh)(PCy$_3$)$_2$ shows an intense absorption band at λ_{max} = 334 nm and a weak low-energy absorption at λ_{max} = 520 nm.

The UV−vis absorption spectra of **6**−**15** are illustrated in Figure 6. The absorption spectra of **6**−**9** feature an intense low-energy absorption band at λ_{max} = 479−513 nm with ϵ_{max} values in excess of 10^3 dm^3 mol^{-1} cm^{-1}, indicating a dipole-allowed electronic transition. The absorption maximum is solvatochromic

Table 3. UV−Visible Absorption Data for *trans*-[Cl(16-TMC)Ru=C=CHR]PF_6 (**1**−**5**), *trans*-[Cl(16-TMC)Ru=C=C=C(C_6H_4X-4)$_2$]PF_6 (**6**−**9**), and *trans*-[Cl(dppm)$_2$M=C=C=C(C_6H_4X-4)$_2$]PF_6 (M = Ru, **10**−**12**; M = Os, **13**−**15**) (in CH_3CN), $RuCl_2$(=CHPh)(PCy_3)$_2$, and $RuCl_2$(=C=CHPh)(PCy_3)$_2$ (in CH_2Cl_2)

complex	λ_{max}, nm (ϵ_{max}/dm^3 mol^{-1} cm^{-1})
1 (R = Ph)	273 (19700), 311 (7360), 351 (590), 464 (68), 585 (38), 644 (37)
2 (R = C_6H_4Cl-4)	277 (21510), 315 (12790), 354 (3250), 470 (78), 578 (48), 638 (46)
3 (R = C_6H_4Me-4)	273 (25040), 311 (10740), 350 (900), 464 (68), 582 (33)
4 (R = C_6H_4OMe-4)	273 (28830), 310 (10130), 365 (570), 465 (71), 585 (37)
5 (R = $CHPh_2$)	237 (22850), 304 (2200), 395 (83), 466 (82), 589 (21, br, sh)
6 (X = H)	258 (14110), 283 (13160), 335 (7390), 479 (20200)
7 (X = Cl)	292 (15360), 335 (9790), 483 (21740)
8 (X = Me)	260 (14780), 291 (12830), 341 (11510), 492 (24430)
9 (X = OMe)	264 (14540), 279 (13370), 382 (17510), 513 (29760)
10 (X = H)	273 (46900), 357 (9010), 506 (17120)
11 (X = Cl)	274 (49940), 366 (12590), 510 (19970)
12 (X = Me)	273 (48370), 374 (14170), 519 (20210)
13 (X = H)	252 (56640), 350 (7330), 468 (22370), 525 (13350, sh)
14 (X = Cl)	252 (57610), 350 (10690), 473 (25210), 527 (13690, sh)
15 (*X* = Me)	252 (68380), 359 (15690), 474 (28400), 527 (23770, sh)
$RuCl_2$(=CHPh)(PCy_3)$_2$	254 (14320), 334 (8060), 520 (360)
$RuCl_2$(=C=CHPh)(PCy_3)$_2$	264 (36440), 306 (34100), 363 (2060), 494 (230), 594 (160)

(e.g., for **6**, λ_{max} = 479 nm in CH_3CN, 488 nm in $CHCl_3$) and red-shifts in energy as the electron-donating ability of the substituent at C_6H_4X-4 increases, except for X = Cl [λ_{max} = 479 nm for **6** (H), 483 nm for **7** (Cl), 492 nm for **8** (Me), 513 nm for **9** (X = OMe)]. This anomaly may be rationalized by the negative inductive and positive mesomeric effects of the chloro substituent. Like **6**−**8**, the UV−vis absorption spectra of **10**−**12** contain an intense low-energy absorption band with ϵ_{max} values in excess of 10^3 dm^3 mol^{-1} cm^{-1} in a similar spectral region, and the λ_{max} value decreases as X changes from Me to Cl and H (λ_{max} = 519, 510, and 506 nm, respectively). Interestingly, the absorption maxima are red-shifted by 1060−1110 cm^{-1} compared with the 16-TMC analogues **6**−**8**. The UV−vis absorption spectra of **13**−**15** show an intense absorption band at λ_{max} = 468−474 nm with a prominent shoulder at 525−527 nm ($\epsilon_{max} \geq 10^3$ dm^3 mol^{-1} cm^{-1}), signifying dipole-allowed electronic transition(s). The shift in the absorption maximum also parallels the trend observed for **6**−**8** and **10**−**12** [λ_{max} = 474 nm for **15** (Me), 473 nm for **14** (Cl), 468 nm for **13** (H)].

Resonance Raman Spectroscopy. Figure 7 shows the resonance Raman spectrum of **6** obtained with 435.7 nm excitation. A similar spectrum was also obtained with 502.9 nm excitation (see Supporting Information). The largest resonance Raman progression is the fundamental and overtone of the nominal $\nu_{C=C=C}$ stretch mode at 1889 and 3786 cm^{-1}, respectively (this nominal $\nu_{C=C=C}$ mode was observed at 1884 cm^{-1} in the IR spectrum). The nominal $\nu_{C=C=C}$ mode at 1889 cm^{-1} also forms weaker combination bands with eight other fundamental Franck−Condon active modes. The resonance Raman shifts and intensities for the Raman bands observed for

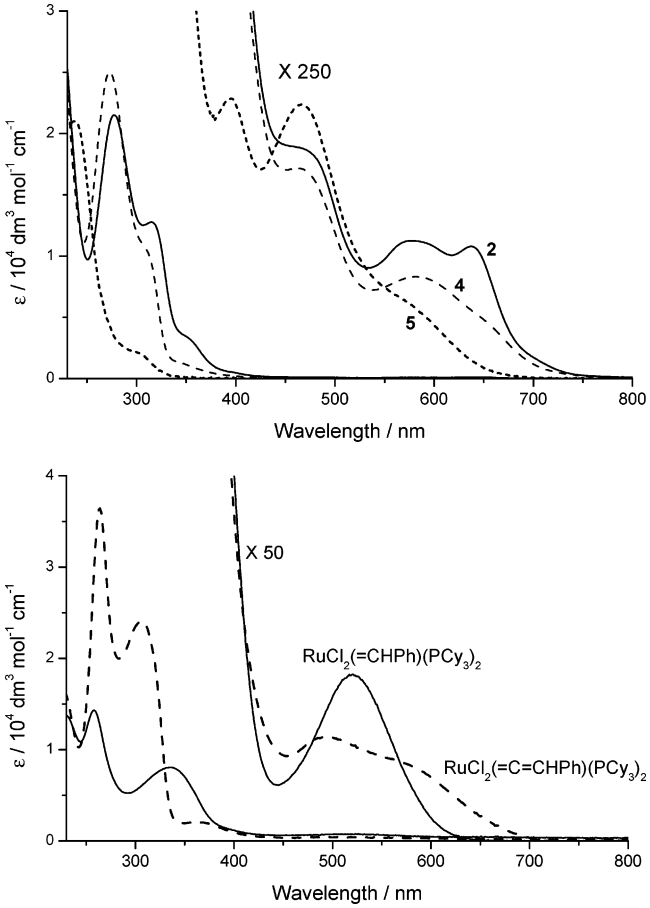

Figure 5. (Top) UV−vis absorption spectra of *trans*-[Cl(16-TMC)Ru=C=CHR]PF_6 (R = C_6H_4Cl-4 (**2**), C_6H_4OMe-4 (**4**), $CHPh_2$ (**5**)) in CH_3CN at 25 °C. (Bottom) UV−vis absorption spectra of $RuCl_2$(=CHPh)(PCy_3)$_2$ and $RuCl_2$(=C=CHPh)(PCy_3)$_2$ in CH_2Cl_2 at 25 °C.

the 435.7 and 502.9 nm spectra together with the absolute Raman cross sections for the nominal $\nu_{C=C=C}$ stretch mode are listed in Table 4.

We simulated the 479 nm absorption band and the resonance Raman intensities of **6** in order to obtain semiquantitative information about the structural changes in the excited state relative to the ground state. The methodology for the resonance Raman intensity analysis is the same as that reported in a number of our previous studies.[31] Table 5 presents the best-fit parameters for the simulations and the vibrational reorganization energies determined from the normal mode displacements. The top of Figure 8 depicts a comparison of the calculated and experimental absorption spectrum and its Gaussian deconvolution. The bottom of Figure 8 represents a comparison of the computed absolute Raman cross sections with the experimental values for the 13 combination bands and overtones as well as the 12 fundamental vibrational modes observed in the resonance Raman spectrum of **6**. The calculated absorption spectrum in Figure 8 exhibits good correlation with the Gaussian deconvolution of the experimental spectrum. Similarly, the calculated absolute Raman

(31) (a) Leung, K. H.; Phillips, D. L.; Mao, Z.; Che, C.-M.; Miskowski, V. M.; Chan, C.-K. *Inorg. Chem.* **2002**, *41*, 2054−2059. (b) Che, C.-M.; Mao, Z.; Miskowski, V. M.; Tse, M.-C.; Chan, C.-K.; Cheung, K.-K.; Phillips, D. L.; Leung, K.-H. *Angew. Chem., Int. Ed.* **2000**, *39*, 4084−4088. (c) Che, C. M.; Tse, M.-C.; Chan, M. C. W.; Cheung, K. K.; Phillips, D. L.; Leung, K.-H. *J. Am. Chem. Soc.* **2000**, *122*, 2464−2468. (d) Leung, K. H.; Phillips, D. L.; Tse, M.-C.; Che, C.-M.; Miskowski, V. M. *J. Am. Chem. Soc.* **1999**, *121*, 4799−4803. (e) Kwok, W. M.; Phillips, D. L., Yeung, P. K.-Y.; Yam, V. W.-W. *J. Phys. Chem. A* **1997**, *101*, 9286−9295.

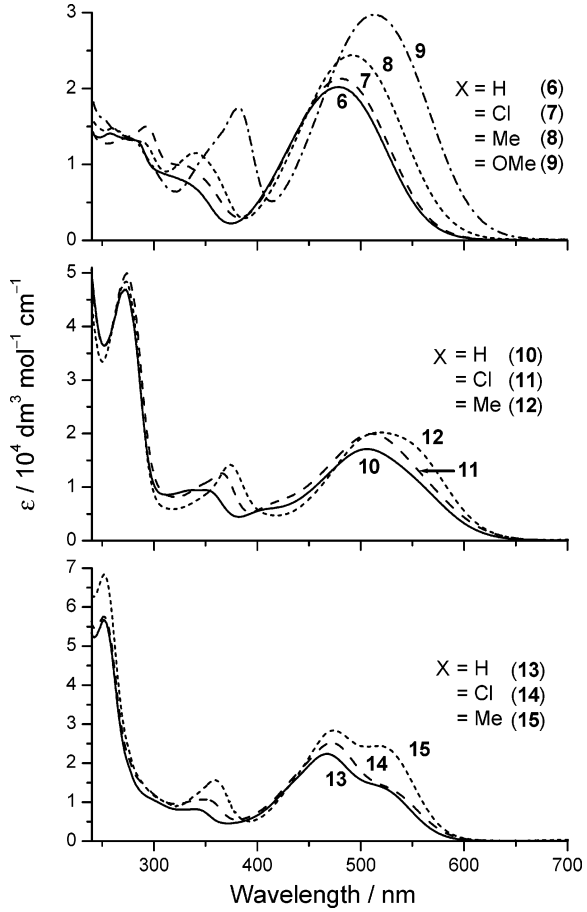

Figure 6. UV−vis absorption spectra of *trans*-[Cl(16-TMC)Ru=C=C=C(C_6H_4X-4)$_2$]PF_6 (**6**−**9**) and *trans*-[Cl(dppm)$_2$M=C=C=C(C_6H_4X-4)$_2$]PF_6 (M = Ru, **10**−**12**; M = Os, **13**−**15**) in CH_3CN at 25 °C.

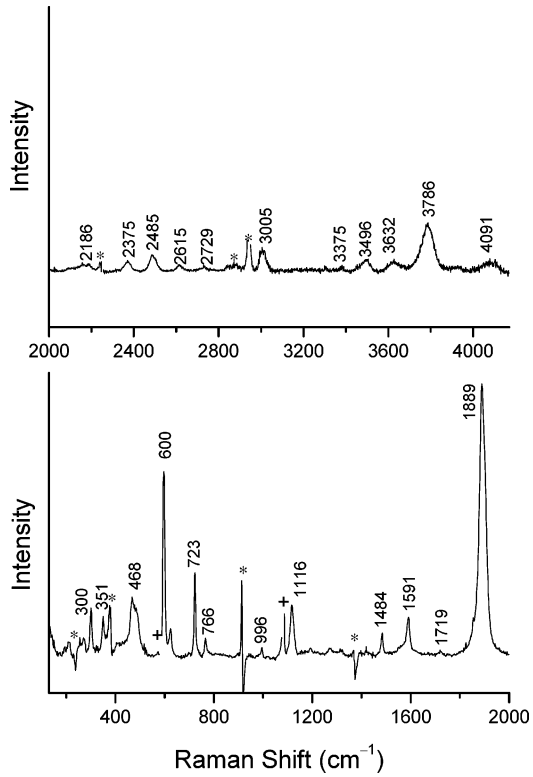

Figure 7. Resonance Raman spectrum of **6** obtained with 435.7 nm excitation wavelength in CH_3CN at 25 °C (solvent and laser subtraction artifacts marked by * and +, respectively).

Table 4. Resonance Raman Bands for **6** in CH_3CN

Raman band	Raman shift[a]/cm^{-1}	relative intensity[b] at 435.7 nm	relative intensity[b] at 502.9 nm
	300	5	3
	351	5	3
	468	7	5
	600	17.5	12
	723	9	6.5
	766	3	4
	996	2	2
	1116	17	11
	1276	2	2
	1484	2.6	3
$\nu_{C=C}$	1591	7	9
$\nu_{C=C=C}$	1889	100	100
600 + 723	1317	1	1
600 + 1116	1719	2	1
$\nu_{C=C}$ + 600	2186	4	4
$\nu_{C=C=C}$ +468	2375	4.5	3.5
$\nu_{C=C=C}$ + 600	2485	7	7
$\nu_{C=C=C}$ + 723	2615	3	3
$\nu_{C=C}$ + 1116	2729	2	
$\nu_{C=C=C}$ + 1116	3005	7	5
$\nu_{C=C=C}$ + 1484	3375	1	
$\nu_{C=C=C}$ + $\nu_{C=C}$	3496	4	
$\nu_{C=C=C}$ + 1116 + 600	3632	3	
2 × $\nu_{C=C=C}$	3786	22	
$\nu_{C=C=C}$ + $\nu_{C=C}$ + 600	4091	5	
absolute Raman cross section	expt.	0.58×10^{-7}	0.69×10^{-7}
for $\nu_{C=C=C}$ (in /Å^2/molecule)	calcd[c]	0.60×10^{-7}	0.65×10^{-7}

[a] Estimated uncertainties are about 4 cm^{-1} for the Raman shifts. [b] Relative intensities are based on integrated areas of Raman bands. Estimated uncertainties are about 5% for intensities greater than 50, 10% for intensities between 10 and 50, and 20% for intensities below 10. [c] Calculated using parameters from Table 5 and model described in text and ref 31.

Table 5. Parameters for Simulations (using Exponential Damping Function) of Resonance Raman Intensities and Absorption Spectrum of **6** in CH_3CN[a]

ground-state vib. freq./cm^{-1}	excited-state vib. freq./cm^{-1}	Δ	vib. reorg. energy/cm^{-1}
300	300	0.783	92
351	351	0.719	91
468	468	0.760	135
600	600	0.932	261
723	723	0.550	109
766	766	0.364	51
996	996	0.210	22
1116	1116	0.520	151
1276	1276	0.200	26
1484	1484	0.193	28
1591	1591	0.350	97
1889	1889	1.060	1061

[a] Total $\lambda_v = 2124$; $E_0 = 19\,200 \pm 100$ cm^{-1}; $M = 1.75 \pm 0.10$ Å; $n = 1.344$; homogeneous broadening, $\Gamma = 780 \pm 80$ cm^{-1} HWHM; inhomogeneous broadening, $G = 250 \pm 50$ cm^{-1} standard deviation.

cross sections show reasonable agreement with experimental counterparts.

The resonance Raman spectrum of **5** was also obtained with 309.1 nm excitation (see Supporting Information). The largest resonance Raman progression is the fundamental of the nominal $\nu_{C=C}$ stretch mode at 1629 cm^{-1} (this $\nu_{C=C}$ mode was observed at 1631 cm^{-1} in the IR spectrum). The nominal $\nu_{C=C}$ mode at 1629 cm^{-1} generates an overtone at 3258 cm^{-1} and similarly affords combination bands with some fundamental Franck−Condon active modes.

Ab Initio Calculations. The ground-state structure of the model complex *trans*-[Cl(NH$_3$)$_4$Ru=C=C=CPh$_2$]$^+$ is depicted in Figure 9 (top), and the optimized structural data are

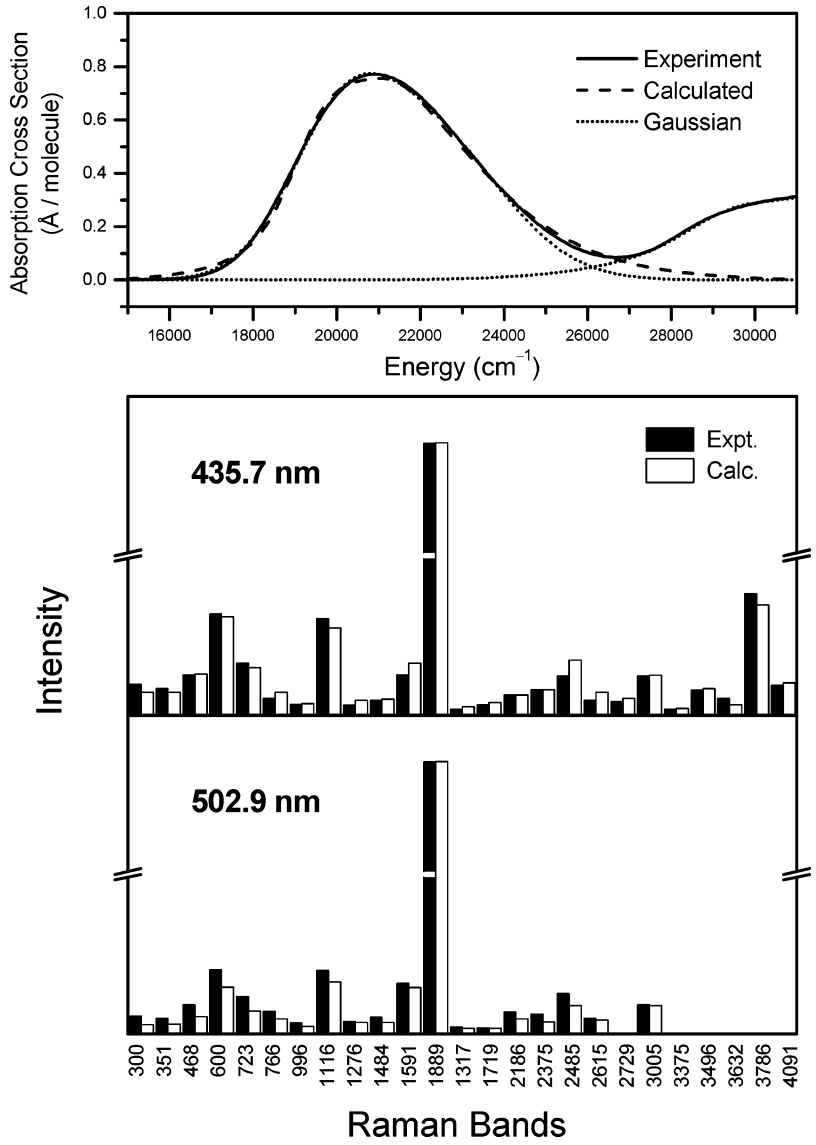

Figure 8. (Top) Comparison of the calculated absorption spectrum with the experimental and Gaussian deconvolution absorption spectra. (Bottom) Comparison of the calculated Raman cross sections with the experimental values observed in the 435.7 and 502.9 nm resonance Raman spectra of **6**. The calculations used the parameters given in Table 5 and the model described in references for the simple exponential decay dephasing description of the solvent.[31]

summarized in the Supporting Information. All the optimized structural data are in satisfactory agreement with the crystal structure of $[Cl(16\text{-TMC})Ru{=}C{=}C{=}CPh_2]^+$ (**6**), except that the calculated C═C═C bond angle is linear. The compositions of the HOMO and LUMO [depicted in Figure 9 (bottom)], together with the Mulliken and natural charges, are listed in the Supporting Information. The major components of the frontier molecular orbitals originate from the orbitals of Ru, C═C═C, and Ph rings, while the total contribution from the orbitals of chloride and amine ligands is less than 10%. In the HOMO, the contributions from Ru, C═C═C, and Ph rings are 23%, 22%, and 49%, respectively, while in the LUMO they are 13%, 48%, and 36%, respectively. We note that along the C═C═C unit, the HOMO contains contribution mainly from the central carbon atom C_β (2.3% for C_α, 15.4% for C_β, 4.2% for C_γ) while the LUMO is mainly composed of participation by the odd-numbered carbon atoms C_α and C_γ (18.0% for C_α, 2.6% for C_β, 27.2% for C_γ). The Mulliken net charges on Ru, C_α, C_β, and C_γ are 0.55, 0.17, −0.72, and 0.04, respectively (the corresponding natural charges[20] are 0.48, −0.07, −0.15, and −0.01, respectively), which signifies that (1) the metal center is more positively charged than the C═C═C unit and (2) C_β is more negatively charged than C_α or C_γ.

Discussion

Nature of Bonding in $[Ru(=C)_nCR_2]$. In this work, we presented the crystal structures of a number of vinylidene− and allenylidene−ruthenium complexes supported by the 16-TMC ligand. The Ru−C_α bonds are slightly longer and the C_α−C_β distances are significantly shorter for the allenylidene complexes. By comparison with acetylide complexes such as *trans*-[Ru(16-TMC)$(C{\equiv}CPh)_2$],[11b] it is apparent from the Ru−C_α and C_α−C_β distances that the bonding character of the allenylidene fragment is intermediate between vinylidene and acetylide, i.e., the C_α−C_β bonds of *trans*-$[Cl(16\text{-TMC})Ru{=}C{=}C{=}CR_2]PF_6$ exhibit partial triple-bond character. In the literature, this has been attributed to the alkynyl mesomer: $M^n{=}C{=}C{=}CR_2 \leftrightarrow M^{n-1}{-}C^+{=}C{=}CR_2 \leftrightarrow M^{n-1}{-}C{\equiv}C{-}C^+R_2$. For example, Dixneuf and co-workers suggested that for *trans*-$[(dppm)_2Ru(=C{=}C{=}C(OMe)CH{=}CPh_2)_2](BF_4)_2$, which features long Ru−

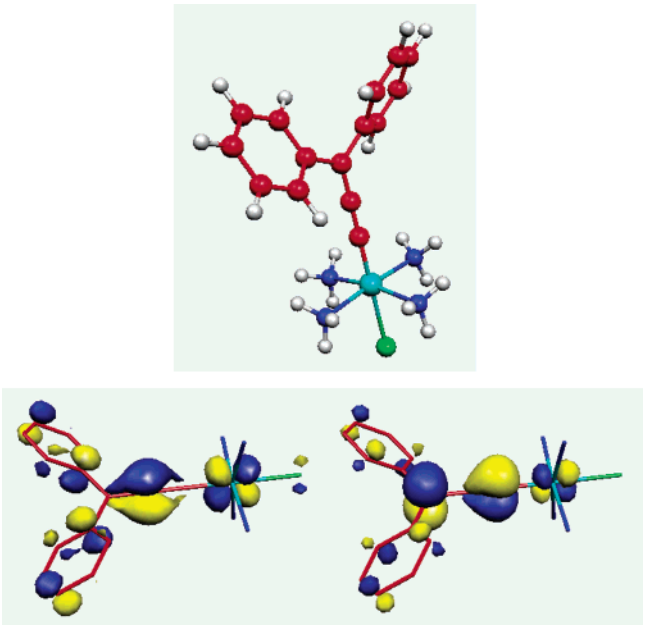

Figure 9. Optimized structure (top), HOMO (left), and LUMO (right) of the model compound $[Cl(NH_3)_4Ru{=}C{=}C{=}CPh_2]^+$.

C_α and $C_\beta{-}C_\gamma$ but short $C_\alpha{-}C_\beta$ distances, the electron-donating OMe group can stabilize the mesomeric forms: $[Ru^+{=}C{=}C{=}C{-}OMe] \leftrightarrow [Ru{-}C{\equiv}C{-}C^+{-}OMe] \leftrightarrow [Ru{-}C{\equiv}C{-}C{=}(^+O)\text{-}Me]$.[6c] Similarly, Bruce et al. rationalized the deviations in bond lengths between $[Ru\{C{=}C{=}CMe(NPh_2)\}(PPh_3)_2(\eta\text{-}C_5H_5)]^+$ and $[Ru\{C{=}C{=}CPh_2\}(PMe_3)_2(\eta\text{-}C_5H_5)]^+$ by proposing that the N lone pair electrons can stabilize the $[Ru(C{\equiv}CCMe{=}NPh_2)]^+$ tautomer.[6b] Tamm et al. reported the allenylidene complex with a tropylium substituent, [CpRu=C=C=C(cycloheptatrienylidene)(PPh_3)]PF_6, and concluded that the cycloheptatrienyl unit can stabilize a positive charge, and thus the $Ru{-}C{\equiv}C{-}CR^+$ mesomeric form is important.[6a]

We conceive that, in this study, the contribution of the $M^{n-1}{-}C{\equiv}C{-}C^+R_2$ form to the $Ru{=}C{=}C{=}CR_2$ bonding in *trans*-[Cl(16-TMC)Ru=C=C=CR_2]PF_6 is less important than that in the phosphine/Cp-stabilized analogues described above and in the literature. First, 16-TMC is an effective σ-donor, and this would destabilize the $M^{n-1}{-}C{\equiv}C{-}C^+R_2$ form. This is supported by the $\nu_{C=C}$ and $\nu_{C=C=C}$ values in this work being the lowest reported for vinylidene− and allenylidene−ruthenium derivatives. Second, complexes **6**−**9** do not contain any heteroatoms or conjugated systems that can stabilize a positive charge on the allenylidene ligand. Third, **6**−**9** are stable in refluxing MeOH, and no reaction is observed between **6** and NaOMe; this is in stark contrast to phosphine-supported cationic congeners such as **10**−**12**, which have been reported to react with strong nucleophiles such as methoxide to afford functionalized alkynyl compounds.[1a] However, **6** does not react with the Lewis acid CF_3COOH, therefore, it appears that the allenylidene ligand in *trans*-[Cl(16-TMC)Ru=C=C=CR_2]PF_6 is not sufficiently electron-rich to exhibit nucleophilic character. At this juncture, we note that accounts of the reactivity of nucleophilic allenylidene ligands have appeared in the literature. Valerga and co-workers reported that $[(Cp^*)(dippe)Ru{=}C{=}C{=}CPh_2]^+$ reacts with H^+ to afford $[(Cp^*)(dippe)Ru{\equiv}C{-}CH{=}CPh_2]^{2+}$, and treatment of $[(Cp^*)(dippe)Ru{=}C{=}C{=}CPhH]^+$ with pyrrole and 2-methylfuran gives $[(Cp^*)(dippe)Ru{=}C{=}CH{-}C(2\text{-pyrrolyl})\text{-}PhH]^+$ and $[(Cp^*)(dippe)Ru{=}C{=}CH{-}C(5\text{-methyl-2-furanyl})\text{-}PhH]^+$, respectively, only when $HBF_4{\cdot}Et_2O$ is present.[3c] Werner and co-workers also reported that the neutral vinylidene complexes $[Cl_2L_2Ru{=}C{=}CRH]$ (L = PCy_3, P^iPr_3; R = Ph, ^{t}Bu) are susceptible to electrophilic attack by H^+ to give $[Cl_2L_2\text{-}Ru{\equiv}C{-}CRH_2]^+$.[3f]

Theoretical calculations also provide information regarding the charge distribution along the $[Ru{=}C{=}C{=}CR_2]$ unit. Esteruelas et al. performed EHT-MO calculations on $[Ru(Cp)(C{=}C{=}CH_2)(CO)(PH_3)]^+$, and the Mulliken atomic net charges on the carbon atoms are −0.36 (C_α), −0.13 (C_β), and −0.05 (C_γ).[32] Auger et al. reported DFT calculations on the model ruthenium cumulene complexes $[Cl(PH_3)_4Ru(=C)_nH_2]^+$ (n = 1−8).[33] In each case, the Mulliken net charge on the metal center is positive while the $(=C)_n$ chain is negatively charged (e.g., for n = 3, Mulliken net charges on Ru, C_α, C_β, and C_γ are 0.60, −0.28, −0.03, and 0.21, respectively). In the ab initio calculations (at MP2 level) performed in this work on the model complex $[Cl(NH_3)_4Ru{=}C{=}C{=}CPh_2]^+$, the Mulliken charges alternate along the C=C=C moiety (for Ru, C_α, C_β, and C_γ = 0.55, 0.17, −0.72, and 0.04, respectively; the corresponding natural charges[20] are 0.48, −0.07, −0.15, and −0.01, respectively). This indicates that like the related calculations described above,[32,33] the metal center is more positive than the C=C=C unit. Interestingly, with respect to the ruthenium−allenylidene interaction, these results are consistent with the polarized $M^{\delta+}[(=C)_2CR_2]^{\delta-}$ description. We note that theoretical calculations for the neutral rhodium vinylidene complex *trans*-[RhCl(=C=CH_2)(PMe_3)$_2$] show that the metal center is more negative than the carbon atom in the Rh=C bond,[3g] but it is clear that Rh(I) is generally more electron-rich than ruthenium in oxidation state ≥2. The alternation of Mulliken charges along the C=C=C unit in $[Cl(NH_3)_4Ru{=}C{=}C{=}CPh_2]^+$, which is not observed in $[Ru(Cp)(C{=}C{=}CH_2)(CO)(PH_3)]^+$ [32] and $[Cl(PH_3)_4\text{-}Ru(=C)_3H_2]^+$,[33] presumably arises because of the use of diphenyl-substituted (C=C=CPh_2) rather than nonsubstituted (C=C=CH_2) allenylidene groups in the calculation.

In $[Cl(NH_3)_4Ru{=}C{=}C{=}CPh_2]^+$, the contributions in the HOMO from Ru, C=C=C, and Ph rings constitutes 94% of the total and the percentage contributions are 23%, 22%, and 49%, respectively. This implies the HOMO is not localized solely on the metal center or allenylidene ligand but is delocalized along the Ru=C=C=CAr_2 unit. This is in accordance with the electrochemical data (see below), which show that the metal ion affects the electrochemical oxidation potential of the M=C=C=CAr_2 unit. On the other hand, the contributions from Ru, C=C=C, and Ph rings add up to 97% of the total for the LUMO (percentage contributions are 13%, 48%, and 36%, respectively), suggesting the LUMO is localized more on the allenylidene ligand and especially the C=C=C unit.

Electrochemical Comparisons. The electrochemical behavior of the allenylidene complexes reported in this work can provide insight into the nature of $M{=}C{=}C{=}CR_2$ bonding. Taking the series where R = Ph (**6**, **10**, and **13**) as an example, the $E_{1/2}$ values of **6** ($E_{1/2}$ = −1.27, 0.64 V) and **10** ($E_{1/2}$ = −0.98, 1.02 V) show that changing the ligand system from N [16-TMC]

(32) Esteruelas, M. A.; Gómez, A. V.; López, A. M.; Modrego, J.; Oñate, E. *Organometallics* **1997**, *16*, 5826−5835.
(33) Auger, N.; Touchard, D.; Rigaut, S.; Halet, J.-F.; Saillard, J.-Y. *Organometallics* **2003**, *22*, 1638−1644.

to P [(dppm)$_2$] donors increases the $E_{1/2}$ values of these two couples by 290 and 380 mV, respectively. Because the equatorial dppm and 16-TMC auxiliaries would influence the oxidation potential of ruthenium through π-back-bonding and/or σ-bonding interactions, such an impact upon the $E_{1/2}$ values suggests that the electrochemical reactions involve the metal ion and are unlikely to be localized solely on the C═C═CPh$_2$ unit. In addition, the difference between the $E_{1/2}$ values of **10** ($E_{1/2}$ = −0.98, 1.02 V) and **13** ($E_{1/2}$ = −1.14, 0.82 V) demonstrate the effect of the metal center. However, the electrochemical reactions do not appear to be purely metal-localized, and this is indicated by the substituent effect of the C$_6$H$_4$X-4 rings upon the $E_{1/2}$ values of the two couples; the variations in $E_{1/2}$ values of both couples are around 200 mV upon changing X from Cl (**7**) to OMe (**9**). Therefore, a reasonable proposal is that the electrochemical reactions occur at the delocalized M═C═C═CR$_2$ unit. To obtain further information regarding the electrochemical reaction of the M═C═C═CR$_2$ unit, we note the following: (1) the difference in $E_{1/2}$ value for the metal-centered Ru(III)/(II) couple between *trans*-[(dppm)$_2$RuCl$_2$]$^{+/0}$ (0.14 V)[34] and [(16-TMC)RuCl$_2$]$^{+/0}$ (−0.60 V)[12c] is 740 mV, which is significantly greater than that between [Cl(16-TMC)Ru═C═C═CPh$_2$]$^+$ and [Cl(dppm)$_2$Ru═C═C═CPh$_2$]$^+$ (290 and 380 mV for the +/0 and 2+/+ couples respectively), (2) the increase in $E_{1/2}$ value for the M(III)/(II) couple of *trans*-[(16-TMC)MCl$_2$]$^{+/0}$ as M changes from Os to Ru is 770 mV, while the difference in $E_{1/2}$ value for *trans*-[(dppm)$_2$MCl$_2$]$^{+/0}$ and [Cl(dppm)$_2$M═C═C═CPh$_2$]$^+$, for M = Ru and Os, is 240 mV[16] and 160/200 (for the +/0 and 2+/+ couples respectively) mV, respectively. These observations are consistent with the notion that the redox couples for the allenylidene−ruthenium (**6**−**12**) and −osmium (**13**−**15**) complexes are not purely metal- or ligand-centered.

Compared with the diphosphine analogue **10** ($E_{1/2}$ = −0.98, 1.02 V), the $E_{1/2}$ values of the two couples for **6** ($E_{1/2}$ = −1.27, 0.64 V) occur at more negative potentials, indicating the ability of the strongly σ-donating 16-TMC ligand to increase electron density at the metal center. The $E_{1/2}$ values of the two couples for the osmium derivative **13** ($E_{1/2}$ = −1.14, 0.82 V) also occur at more negative potentials than **10**, as would be expected since osmium has a lower oxidation potential.

With regard to the assignment of the two couples, it is interesting to compare the redox couples of *trans*-[(TMC)ClRuL]$^{n+}$, which have been extensively studied.[12b,c] The 2+/+ couples of *trans*-[(16-TMC)ClRu^{III}Cl]$^+$, *trans*-[(14-TMC)ClRu^{IV}═O]$^+$, and *trans*-[(14-TMC)ClRu^{II}−N≡CCH$_3$]$^+$ occur at 1.16, 1.10, and 0.15 V, respectively. The couples of *trans*-[(16-TMC)ClRu═C═C═CR$_2$]$^{2+/+}$ (**6**−**9**) in this work (0.49−0.70 V) exist between those of [(16-TMC)ClRu═O]$^{2+/+}$ and [(14-TMC)ClRu−N≡CCH$_3$]$^{2+/+}$, implying that the ease of oxidation for *trans*-[(16-TMC)ClRu═C═C═CR$_2$]$^+$ is between those of [Ru^{II}−N≡CCH$_3$]$^+$ and [Ru^{IV}═O]$^+$. We suggest that the other reversible wave of **6**−**9** (−1.19 to −1.42 V) corresponds to the *trans*-[(16-TMC)ClRu═C═C═CR$_2$]$^{+/0}$ couple, which is generally more cathodic than that of *trans*-[(16-TMC)ClRuCl]$^{+/0}$ (−0.60 V). This is in agreement with the above observation that [Cl−Ru═C═C═CR$_2$]$^+$ is more electron-rich than the *trans*-[Cl−Ru^{III}−Cl]$^+$ moiety.

Insight from Electronic and Resonance Raman Spectroscopy. The vinylidene complexes **1**−**4** show similar absorption patterns in the UV region ($\lambda_{max} \leq$ 310 nm, $\epsilon_{max} \geq 10^4$ dm^3 mol^{-1} cm^{-1}), and these are clearly different from **5**. As the main difference between **1**−**4** and **5** is the nature of the vinylidene ligand, we suggest that these high-energy transition bands involve the vinylidene moiety. Support for this assignment is provided by the resonance Raman spectrum of **5** obtained with 309.1 nm excitation, which shows large resonance Raman enhancement in the fundamental of the nominal $\nu_{C=C}$ stretch mode at 1629 cm^{-1}. This indicates that the electronic transition involves large structural distortion of the vinylidene unit.

The UV−vis absorption spectra of the vinylidene complexes **1**−**5** show weak absorptions in the low-energy region (λ_{max} = 460−640 nm), with ϵ_{max} values below 10^2 dm^3 mol^{-1} cm^{-1}. We propose that these absorption bands are likely to be d−d transitions in nature. The alternative assignment to spin-forbidden analogues of the intense UV electronic transitions is unfavored because (1) the excessively large S−T splitting is unreasonable and (2) such spin-forbidden transitions in Ru complexes are expected to be substantially weaker compared to the visible absorption bands observed in this study. For a Ru(IV)−ligand multiple bond (d^4) formalism, there emerges an obvious assignment to $d_{xy} \rightarrow (d_{xz}, d_{yz})$ transitions. The theoretical framework for interpreting such transitions and the nature of the ground states have been established for metal mono-oxo analogues.[35] Interestingly, the spin-allowed $d_{xy} \rightarrow (d_{xz}, d_{yz})$ transition in d^4 Ru(IV)═O complexes occurs at a similar spectral region to the proposed d−d transitions of the vinylidene complexes **1**−**5**, namely, λ_{max} 460−600 nm.[12b] A complication for the compounds in the present study is that the d_{xz} and d_{yz} orbitals are not degenerate in energy; in particular, this may account for the complexity of the ∼600 nm absorption of **2**.

The UV−vis absorption spectrum of the vinylidene complex RuCl$_2$(═C═CHPh)(PCy$_3$)$_2$ shows similar absorption patterns to those of **1**−**4**. As the PCy$_3$ ligand is also optically transparent in this region, the nature of the electronic transitions for *trans*-[Cl(16-TMC)Ru═C═CHAr]PF$_6$ and RuCl$_2$(═C═CHPh)(PCy$_3$)$_2$ are likely to be similar. The corresponding alkylidene complex RuCl$_2$(═CHPh)(PCy$_3$)$_2$, which differs by one cumulene carbon unit, also displays low-energy absorption bands at similar energies and extinction coefficients to those of RuCl$_2$(═C═CHPh)(PCy$_3$)$_2$. From the viewpoint that the differences between the high-energy absorption spectra of RuCl$_2${(═C)$_n$HPh}(PCy$_3$)$_2$ (n = 1 and 2) are due to modification of the cumulene ligand, we suggest that perturbation of the metal-centered d−d transition would be less dramatic, since the Ru−C$_\alpha$ distance in RuCl$_2$(═CHR)(PCy$_3$)$_2$ (1.838(3)[8f] and 1.851(21)[8g] Å for R = C$_6$H$_4$Cl-4 and CH═CPh$_2$, respectively) and RuCl$_2$(═C═CHPh)(PCy$_3$)$_2$ (1.761(2) Å)[14] are comparable. Thus, the ruthenium−carbon bonding interaction in Ru═CHR and Ru═C═CHR are envisaged to be alike in these complexes. Incidentally, one would expect such weak visible band(s) to be present in the absorption spectra of **6**−**9**, but they are presumably obscured by the intense electronic transition at λ_{max} = 479−513 nm.

The UV−vis absorption spectra of the allenylidene−ruthenium complexes bearing 16-TMC (**6**−**9**) and dppm (**10**−**12**) feature an intense low-energy absorption band at λ_{max} =

(34) Champness, N. R.; Levason, W.; Pletcher, D.; Webster, M. *J. Chem. Soc., Dalton Trans.* **1992**, 3243−3247.

(35) Miskowski, V. M.; Gray, H. B.; Hopkins, M. D. *Adv. Transition Met. Coord. Chem.* **1996**, *1*, 159−186.

479−513 and 506−519 nm, respectively, with ϵ_{max} values in excess of 10^3 dm^3 mol^{-1} cm^{-1}. The UV−vis absorption spectra of the allenylidene−osmium dppm complexes **13**−**15** also contain an intense absorption at λ_{max} = 468−474 nm with a prominent shoulder near 525−527 nm ($\epsilon_{max} \geq 10^3$ dm^3 mol^{-1} cm^{-1}). It has been suggested by Tamm et al. that the electronic absorption associated with [CpRu=C=C=C(cycloheptatrienylidene)(PPh$_3$)]PF$_6$ (λ_{max} = 496−601 nm) is due to charge-transfer excitation represented by the resonance structures Ru$^+$=C=C=CR$_2$ ↔ Ru−C≡C−C$^+$R$_2$.[6a] In this work, we found that the absorption maximum of *trans*-[Cl(16-TMC)Ru=C=C=C(C$_6$H$_4$X-4)$_2$]PF$_6$ is sensitive to the nature of the solvent (e.g., λ_{max} = 479 nm in CH$_3$CN, 488 nm in CHCl$_3$ for **6**). The absorption maximum red-shifts in energy as the electronic-donating affinity of the C$_6$H$_4$X-4 ring system increases, which is consistent with charge transfer from allenylidene to ruthenium. The general red shift of the absorption maximum (ca. 1100 cm^{-1}) from *trans*-[Cl(16-TMC)Ru=C=C=C(C$_6$H$_4$X-4)$_2$]PF$_6$ (**6**−**8**) to *trans*-[Cl(dppm)$_2$Ru=C=C=C(C$_6$H$_4$X-4)$_2$]PF$_6$ (**10**−**12**) provides useful information for spectral assignment purposes. For an electronic transition involving ligand-to-metal charge transfer (LMCT), the π-back-bonding between Ru(d_π) orbitals and the phosphine ligands would decrease the electron density around Ru to give a red shift. Furthermore, this assignment is in accordance with the observed blue shift in λ_{max} from *trans*-[Cl(dppm)$_2$Ru=C=C=C(C$_6$H$_4$X-4)$_2$]PF$_6$ (**10**−**12**) to the Os analogues (**13**−**15**), which would be expected for an LMCT transition upon descending the periodic table. Nevertheless, it is apparent that the participation of the metal is small compared to a pure LMCT transition. For example, the energy difference between the λ_{max} of *trans*-[Cl(dppm)$_2$M=C=C=CPh$_2$]PF$_6$ for M = Ru (506 nm) and Os (468 nm) is 1605 cm^{-1}, while the p_π(Cl)-to-d_π(M) LMCT transitions of *trans*-[Ru^{III}(en)$_2$Cl$_2$]$^+$ (λ_{max} = 343 nm) and *trans*-[Os^{III}(en)$_2$Cl$_2$]$^+$ (λ_{max} = 284 nm) show an energy difference of 6056 cm^{-1}.[17a] Moreover, it is evident from the resonance Raman spectroscopic data that the transition involves substantial intraligand $\pi \rightarrow \pi^*$ character. We therefore assign the intense low-energy absorption band of **6**−**15** to a metal-perturbed intraligand transition with some allenylidene-to-metal LMCT character.

Characterization by resonance Raman spectroscopy (Table 4) showed that the 479−513 nm charge-transfer bands originate from a transition that is associated with the Ru=C=C=C moiety. By simulating the 479 nm absorption band and the resonance Raman intensities of **6**, it was found that the nominal $\nu_{C=C=C}$ stretch mode accounts for approximately 50% of the total vibrational reorganization energy, which indicates that the absorption band is strongly coupled to the allenylidene ligand. Furthermore, the reorganization of this ligand in the excited state is accompanied by partial reorganization of the Ru=C and Ru−N (of 16-TMC) fragments (Franck−Condon active modes below 1000 cm^{-1}). In other words, significant interaction exists between the Ru center and the C=C=C moiety in the excited state. It is noteworthy that from our results and calculations the contribution from the $\nu_{C=C}$ stretch mode associated with the phenyl units to the total vibrational reorganization energy is only 97 cm^{-1}, which is less than 10% of the nominal $\nu_{C=C=C}$ contribution (1061 cm^{-1}) (Table 5). This means that the contribution from the phenyl groups to the reorganization energy of the 479 nm electronic transition is minor and signifies that electronic communication between Ru and the peripheral phenyl rings in the excited state is small.

General Remarks. Metal−carbon double-bonded complexes are conventionally categorized as Fischer- or Schrock-type. The Fischer carbene description involves coordination of a neutral carbene ligand to low-valent metal ion through σ- and π-back-bonding interactions. The Schrock alkylidene nomenclature entails a polarized M=C bond ($1\sigma + 1\pi$) with electronic charge localized on the carbon atom. Because of the strong covalent character of a metal−carbon double bond, it is often difficult to clearly distinguish between Fischer and Schrock M=C species. Moreover, the distinction between such bonding descriptions becomes rather ambiguous in the case of ruthenium−vinylidene and −allenylidene derivatives. In the literature,[3−5] the metal oxidation state in such compounds are generally assigned as II, which implies that the vinylidene and allenylidene ligands are neutral (i.e., Fischer description). However, the Grubbs catalyst RuCl$_2$(=CHR)(PCy$_3$)$_2$ and its congeners are often regarded as alkylidene complexes.[8]

In this work, a definitive assignment of the Ru oxidation state in *trans*-[Cl(16-TMC)Ru=C=CHR]PF$_6$ and *trans*-[Cl(16-TMC)-Ru=C=C=CR$_2$]PF$_6$ may be inappropriate given the strong covalency of the Ru=C=C=CR$_2$ bonding interaction. However, it is interesting to note that the proposed d−d transition for the vinylidene complexes *trans*-[Cl(16-TMC)Ru=C=CHR]PF$_6$ (**1**−**5**) occurs at a similar spectral region as the spin-allowed $d_{xy} \rightarrow (d_{xz}, d_{yz})$ transition for d^4 Ru(IV)=O complexes. We suggest that the use of strongly σ-donating ligands such as 16-TMC can facilitate stabilization of species of the M$^{\delta+}$[(=C)$_n$-CR$_2$]$^{\delta-}$ type with respect to the ruthenium−cumulene interaction. Our spectroscopic results signify that the low-energy electronic transition associated with *trans*-[Cl(L$_4$)M=C=C=CR$_2$]$^+$ for **6**−**15** involves a degree of charge transfer from allenylidene to metal. Complexes **6**−**9** bearing 16-TMC are inert toward nucleophilic attack by methoxide, which implies that the contribution of the M^{n-1}−C≡C−C$^+$R$_2$ form to the Ru=C=C=CR$_2$ bonding in *trans*-[Cl(16-TMC)Ru=C=C=CR$_2$]PF$_6$ is not important. The Mulliken and natural population analyses in the ab initio calculations also indicate that the Ru center is more positively charged than the C=C=C chain. Overall, since the 16-TMC- and dppm-ligated allenylidene complexes are spectroscopically and electrochemically alike (bearing in mind that the inability of dppm ligands to stabilize cationic ruthenium centers at high oxidation states is well established), it may be appropriate to consider the allenylidene ligand in these derivatives as neutral, although we favor the polarized Ru$^{\delta+}$[(=C)$_2$-CR$_2$]$^{\delta-}$ description for complexes such as **6**.

The apparent similarities between the electronic transitions associated with the Grubbs alkylidene complex RuCl$_2$(=CHPh)-(PCy$_3$)$_2$, RuCl$_2$(=C=CHPh)(PCy$_3$)$_2$, and *trans*-[Cl(16-TMC)-Ru=C=CHPh]PF$_6$ indicate that the Ru(=C)$_n$CR$_2$ interactions in these three systems are comparable. On the basis of the resonance Raman studies on complex **6**, there is significant delocalization within the linear Ru=C=C=C unit in the charge-transfer (presumably intraligand and allenylidene-to-Ru) excited state. Because the spectroscopic and electrochemical properties of *trans*-[Cl(L$_4$)M=C=C=CR$_2$]$^+$ show close resemblance for M = Ru and Os as well as for L$_4$ = tetraamine and (dppm)$_2$, the bonding description postulated here is expected to be generally applicable to these allenylidene complexes.

Acknowledgment. This work was supported by the Research Grants Council of the Hong Kong SAR, China to C.M.C. (HKU 7077/01P), and The University of Hong Kong Foundation for Educational Development and Research. We thank Dr. B.-H. Xia and Ms. P. Y. Chan for technical assistance regarding the theoretical calculations, and we are grateful to the reviewers for helpful comments and suggestions.

Note Added after ASAP Publication: In the version published on the Web 1/30/2004, the cathodic current in Figure 4 was displayed upward and the anodic current was displayed downward. Figure 4 has been redisplayed with the cathodic current directed downward and the anodic current directed upward (according to Wong, K.-Y.; Che, C.-M.; Anson, F. C. *Inorg. Chem.* **1987**, *26*, 737−741) in the version published 2/4/2004. The final Web version and the print version are correct.

Supporting Information Available: CIF and crystallography data for **1**, **5**, **6**, and **8**; perspective view of the cation in **8**; ^{1}H and $^{13}C\{^{1}H\}$ NMR spectra of **6**; resonance Raman spectra of **5** and **6** (obtained with 309.1 and 502.9 nm excitation wavelength respectively) in CH_3CN at 25 °C; supplementary characterization data; tables of selected structural parameters, partial molecular orbital compositions, and the associated Mulliken and natural charges for the optimized structure of the model complex *trans*-$[Cl(NH_3)_4Ru{=}C{=}C{=}CPh_2]^+$, plus illustrations of selected molecular orbitals. This material is available free of charge via the Internet at http://pubs.asc.org.

JA0380648